

1 **Simulated Hydrologic Response to Projected Changes in Precipitation and**
2 **Temperature in the Congo River Basin**

3 Noel Aloysius^{1,2} and James Saiers¹

4 ¹ School of Forestry and Environmental Studies, Yale University, New Haven,
5 Connecticut, USA

6 ² now at Department of Food, Agriculture & Biological Engineering and

7 Aquatic Ecology Laboratory, Department of Evolution, Ecology and Organismal
8 Biology

9 Ohio State University, Columbus, Ohio, USA

10

11

12

13 **Abstract**

14 Despite their global significance, the impacts of climate change on water resources and
15 associated ecosystem services in the Congo River Basin (CRB) have been understudied.
16 Of particular need for decision makers is the availability of spatial and temporal
17 variability of runoff projections. Here, with the aid of a spatially explicit hydrological
18 model forced with precipitation and temperature projections from 25 global climate
19 models (GCMs) under two greenhouse gas emission scenarios, we explore the variability
20 in modeled runoff in the near (2016-2035) and mid (2046-2065) century. We find that
21 total runoff from the CRB is projected to increase by 5% [-9%; 20%] (mean [min and
22 max] across model ensembles) over the next two decades and by 7% [-12%; 24%] by
23 midcentury. Projected changes in runoff from sub-watersheds distributed within the CRB
24 vary in magnitude and sign. Over the equatorial region and in parts of northern and
25 southwestern CRB, most models project an overall increase in precipitation and,
26 subsequently, runoff. A simulated decrease in precipitation leads to a decline in runoff
27 from head-water regions located in the northeastern and southeastern CRB. Climate
28 model selection plays an important role in future projections, for both magnitude and
29 direction of change. The multi-model ensemble approach reveals that precipitation and
30 runoff changes under business-as-usual and avoided greenhouse gas emission scenarios
31 (RCP8.5 vs. RCP4.5) are relatively similar in the near-term, but deviate in the mid-term,
32 which underscores the need for rapid action on climate change adaptation. Our
33 assessment demonstrate the need to include uncertainties in climate model and emission
34 scenario selection during decision making processes related to climate change mitigation
35 and adaptation.

36 **1. Introduction**

37 Sustainable management of water resources for food production, supply of safe
38 drinking water, and provision of adequate sanitation presents immense challenges in
39 many countries of Central Africa where the Congo River Basin (CRB) is located [*IPCC*,
40 2014; *UNEP*, 2011; *World Food Program*, 2014]. The economies of the nine countries
41 that share the waters of the CRB are agriculture-based [*World Bank Group*, 2014] and,
42 therefore, are vulnerable to the impacts of climate change. Despite the abundant water
43 and land resources and favorable climates, the basin countries are net importers of staple
44 food grains and are far behind in achieving Millennium Development Goals [*Bruinsma*,
45 2003; *Molden*, 2007; *UNEP*, 2011]. Appropriation of freshwater resources is expected to
46 grow in the future as the CRB countries develop and expand their economies. At the
47 same time, climate change related risks associated with water resources will also increase
48 significantly [*IPCC*, 2014].

49 Historical, present and near-future greenhouse gas emissions in the CRB countries
50 constitute a small fraction of global emissions; however, the impacts of climate change
51 on water resources are expected to be severe due to the region's heavy reliance on natural
52 resources (e.g. agriculture and forestry) [*Collier et al.*, 2008; *DeFries and Rosenzweig*,
53 2010; *Niang et al.*, 2014]. The limited adaptation capacity in the CRB region is expected
54 to cause severe water and food security challenges, which, in turn, can lead to ecosystem
55 degradation and increased greenhouse gas emissions [*Gibbs et al.*, 2010; *IPCC*, 2014;
56 *Malhi and Grace*, 2000].

57

58 Strategies for addressing stresses on CRB water resources, including revival of
59 rural economies (largely agriculture based), achieving millennium development goals and
60 environmental conservation, would benefit from detailed information on the spatial and
61 temporal variability of water balance components under different climate projection
62 pathways. The effect of climate change on water resources can be investigated by
63 incorporating climate change projections (e.g. precipitation and temperature) in
64 simulation models that reliably represent the spatial and temporal variability of CRB's
65 hydrology. Such a framework could be applied to project changes in storage and runoff,
66 and hence freshwater availability, under different socioeconomic pathways that affect
67 climate trajectories.

68 A predictive framework of the CRB's hydrology is hindered by insufficient data
69 and too few evaluations of models against available data [*Beighley et al., 2011; Wohl et*
70 *al., 2012*]. Basin scale water budgets estimated from land-based and satellite-derived
71 precipitation datasets reveal significantly different results, and modeled runoff shows
72 only qualitative agreement with corresponding observations [*Alsdorf et al., 2016;*
73 *Beighley et al., 2011; Lee et al., 2011; Schuol et al., 2008*]. *Tshimanga and Hughes*
74 [2012; 2014] recently developed a semi-distributed hydrologic model capable of
75 simulating runoff in CRB. This work crucially identified approaches suitable for
76 approximating runoff generation at the basin scale, although the spatial resolution of the
77 model predictions is rather coarse for supporting regional water management and
78 regional-planning efforts. These regional planning efforts must take into account
79 variability and uncertainties stemming from climate-model selection and projected

80 greenhouse gas emissions, but, with respect to freshwater runoff projections for the CRB,
81 these issues have been inadequately addressed.

82 The goals of this study are to i) develop a spatially explicit hydrology model that
83 uses downscaled output from general circulation models (GCMs) and is suitable for
84 simulating the spatiotemporal variability of runoff in the CRB; ii) test the ability of the
85 hydrological model to reproduce historical data on CRB river discharges using both
86 observed and GCM-simulated climate fields; (iii) quantify the sensitivity and uncertainty
87 of modeled runoff projections to GCM selection; (iv) use the hydrologic model with
88 individual GCMs and multi-GCM ensembles to project near-term (2016-2035) and mid-
89 term (2046-2065) changes in runoff for two greenhouse-gas emission scenarios. We
90 focus on the runoff projections because streams and rivers will serve as the primary
91 sources of freshwater targeted for human appropriation [*Burney et al., 2013; Molden,*
92 2007].

93 We find that a hydrologic model that is forced with bias-corrected and
94 downscaled outputs from an ensemble of 25 GCMs and two emission projects a
95 considerable range in precipitation and runoff, and that runoff projections are highly
96 sensitive to GCM forcing. The multi-model mean (MM, un-weighted average of all
97 GCMs) and the select-model mean (SM, selected GCMs based on performance in the
98 historical period and representation of certain attributes in the climate system) project a
99 1-3% increase in precipitation (20mm – 45mm) and a 4-9% increase in total runoff
100 (15mm-34mm) within the CRB in the near-term (2016-2035) relative to reference period
101 (1985-2005) for MM and SM, respectively. In the mid-term (2036-2065), on the other
102 hand, projections are GCM and emission-scenario dependent, with the high emission

103 RCP8.5 scenario showing the highest increases in precipitation (2-5%, 30mm – 70mm)
104 and runoff (7-14%, 25mm – 50mm) for MM and SM, respectively. Modeled projections
105 also exhibit substantial inter-model variability with projected changes varying between
106 -3% and 9% for precipitation and -12% and 24% for total runoff from the CRB between
107 the mitigation and business-as-usual greenhouse gas emission scenarios. Regionally, both
108 MM and SM project decreasing precipitation and runoff in parts of southern and northern
109 headwater regions of the CRB.

110 **2. Materials and Methods**

111 ***2.1 The Congo River Basin***

112 The Congo River Basin, with a drainage area of 3.7 million km², is the second
113 largest in the world by area and discharge (Figure 1, average discharge of ~41,000 m³s⁻¹)
114 [Runge, 2007]. The basin extends from 9°N to 14°S, while the longitudinal extent is 11°E
115 to 35°E. Nine countries share the water resources of the basin. Nearly a third of the basin
116 area lies north of the equator. Due to its equatorial location, the basin experiences a range
117 of climate regimes. The northern and southern parts have strong dry and wet seasons,
118 while the equatorial region has a bimodal rainy season [Bultot and Griffiths, 1972]. Much
119 of the rain in the northern and southern CRB occurs in Jun-Jul-Aug (JJA) and Dec-Jan-
120 Feb (DJF), respectively. The primary and secondary rainy seasons in the equatorial
121 region are Sep-Oct-Nov (SON) and Mar-Apr-May (MAM, see Bultot and Griffiths
122 [1972] and Supplemental Information (SI) Figure S1). The mean annual precipitation is
123 about 1,500 mm. Rainforests occupy nearly 45% of the basin and are minimally disturbed
124 compared to the Amazon and Southeast Asian forests [Gibbs et al., 2010; Nilsson et al.,
125 2005]. Grassland and savannah ecosystems, characterized by the presence of tall grasses,

126 closed-canopy woodlands, low-trees and shrubs, occupy another 45% [Adams *et al.*,
127 1996; Bartholomé and Belward, 2005; Hansen *et al.*, 2008; Laporte *et al.*, 1998]. Water
128 bodies (lakes and wetlands) occupy nearly 2% of the area and are concentrated mostly in
129 the southeastern and western equatorial parts of the CRB (Figure 1). Soils of the CRB
130 vary from highly weathered and leached Ultisols to Alfisols, Inceptisols and Oxisols
131 [FAO/IIASA, 2009; Matungulu, 1992]. Most soils are deep and well-drained, but they are
132 very acidic, deficient in nutrients, have low capacity to supply potassium and exhibit a
133 low cation exchange capacity [Matungulu, 1992].

134 In order to compare regional patterns in precipitation and runoff, we divided the
135 basin into four regions: i) Northern Congo (NC), ii) Equatorial Congo (EQ), iii)
136 Southwestern Congo (SW), and iv) Southeastern Congo (SE). The EQ region covers most
137 of the rainforest. The SE region consists of numerous interconnected lakes and wetlands.
138 Most of the CRB's population is concentrated in the NC, SE and SW regions [Center for
139 International Earth Science Information Network (CIESIN) Columbia University *et al.*,
140 2005].

141 ***2.2 Hydrologic model for the Congo River Basin***

142 We used a physically based, semi-distributed watershed-scale model that operates
143 at a daily time step [Arnold *et al.*, 1998; Neitsch *et al.*, 2011]. The hydrological processes
144 simulated include evapotranspiration, infiltration, surface and subsurface flows,
145 streamflow routing and groundwater recharge. The model has been successfully
146 employed to simulate river basin hydrology under wide variety of conditions and to
147 investigate climate change effects on water resources [Faramarzi *et al.*, 2013; Krysanova

148 *and White, 2015; Schuol et al., 2008; Trambauer et al., 2013; van Griensven et al.,*
149 *2012].*

150 We delineated 1,575 watersheds within the CRB based on topography [*Lehner et*
151 *al., 2008*]. Watershed elevations vary between 15 m and 2,700 m with a mean value of
152 680 m above mean sea level. Each watershed consists of one stream section, where near-
153 surface groundwater flow and overland flow accumulate before being transmitted through
154 the stream channel to the watershed outlet. Watersheds are further divided into
155 Hydrologic Response Units (HRUs) based on land cover (16 classes, *Bartholomé and*
156 *Belward [2005]*), soils (150 types, *FAO/IIASA [2009]*) and topography. The runoff
157 generated within each watershed is routed through the stream network using the variable
158 storage routing method. The average watershed size and the number of HRUs within each
159 watershed are 2,300 km² and 5, respectively. We also included wetlands and lakes as
160 natural storage structures that regulate the hydrological fluxes at different locations
161 within CRB (Figure 1). Detailed information is not available for the all the lakes;
162 therefore, we incorporated the largest 16 lakes (SI Table S1).

163 Runoff, estimated for each HRU and aggregated at the watershed level, is
164 generated via three pathways: overland flow, lateral subsurface flow through the soil
165 zone and release from shallow groundwater storage. The Curve Number and a kinematic
166 storage routing methods are used to simulate overland and lateral subsurface flows, and a
167 nonlinear storage-discharge relationship is used to simulate groundwater contribution
168 (see *Arnold et al. [1998]; Neitsch et al. [2011]* and SI). A power law relationship is
169 employed to simulate the lake area-volume-discharge (see SI and *Neitsch et al. [2011]*).
170 The potential evapotranspiration is estimated using the temperature-based Hargreaves

171 method [Neitsch *et al.*, 2011]. The actual evapotranspiration is estimated based on
172 available soil moisture and the evaporative demand (i.e. potential evapotranspiration) for
173 the day. Additional details on model development and calibration are provided in the
174 Supplementary Information.

175 ***2.3 Model simulation of historical hydrology with observed climate forcings***

176 We ran the hydrology model for the period 1950-2008. Estimates of observed
177 daily precipitation, and minimum and maximum temperatures needed to calculate
178 potential evapotranspiration were obtained from the Land Surface Hydrology Group at
179 Princeton University [Sheffield *et al.*, 2006]. In addition, measured monthly stream flows
180 were obtained at 30 gage locations (Figure 1) that had at least 10 years of records [Global
181 Runoff Data Center., 2011; Lempicka, 1971; Vorosmarty *et al.*, 1998].

182 The model was calibrated using observed streamflows for the period 1950-1957 at
183 20 locations. The number of model parameters estimated by calibration varied from 10 to
184 13, depending on the location of flow gages (e.g. gages with lakes within their catchment
185 area have more parameters). The calibration involved minimizing an objective function
186 defined as the sum-of-squared errors between observed and simulated monthly average
187 total discharge, baseflows (estimated by applying a baseflow separation method Nathan
188 and McMahon [1990]) and water yield. The Gauss-Marquardt-Levenberg algorithm as
189 implemented in a model independent parameter estimation tool [Doherty, 2004] was used
190 to adjust the fitted parameters and minimize the objective function. Parameter estimation
191 was done in two stages. First, parameters for the watersheds in the upstream gages were
192 estimated. Then the parameters for the downstream gages were estimated. To test the
193 calibrated model, simulated stream flows were compared to stream flows measured at the

194 same 20 locations, but during a period outside of calibration (i.e., 1958-2008), as well as
195 at 10 additional locations that were not used in the calibration.

196 ***2.4 Hydrologic Simulations with Simulated Climate Forcing***

197 Historical climate simulations for the period 1950-2005 and climate projections
198 to 2065 for two greenhouse gas emission scenarios (Representative Concentration
199 Pathway – RCP), mid-range mitigation emission (RCP4.5) and high emission (RCP8.5),
200 were used to drive the hydrologic model. The RCP4.5 scenario employs a range of
201 technologies and policies that reduce greenhouse gas emissions and stabilize radiative
202 forcing at 4.5 W m^{-2} by 2100, whereas the RCP8.5 is a business-as-usual scenario, where
203 greenhouse gas emissions continue to increase and radiative forcing rises above 8.5 Wm^{-2}
204 [Moss *et al.*, 2010; Taylor *et al.*, 2012]. We used monthly precipitation and temperature
205 outputs provided by 25 GCMs (Table 1) for the Fifth Assessment (CMIP5) of the
206 Intergovernmental Panel on Climate Change (IPCC).

207 GCM outputs may exhibit biases in simulating regional climate. These biases,
208 which are attributable to inadequate representation of physical processes by the models,
209 prevent the direct use of GCM output in climate change studies [Randall *et al.*, 2007;
210 Salathé Jr *et al.*, 2007; Wood *et al.*, 2004]. Hydrological assessments that use GCM
211 computations as input inherit the biases [Salathé Jr *et al.*, 2007; Teutschbein and Seibert,
212 2012]. To mitigate this problem, we implemented a statistical method [Li *et al.*, 2010] to
213 bias-correct the monthly historical precipitation and temperature fields. In brief, the
214 method employs a quantile-based mapping of cumulative probability density functions
215 for monthly GCM outputs onto those of gridded observations in the historical period. The
216 bias correction is extended to future projections as well. The observed data used in the

217 modeling and bias-correction has some limitations. That is, the number of precipitation
218 gages decreased over the period from 1950 to 1990, and the density of the gages is sparse
219 compared to the size of the river basin (see Section 3.4 and SI). However, we assumed
220 that the available ground-based observations combined with satellite-based and reanalysis
221 data adequately captured the spatiotemporal variability in precipitation. Studies by
222 *Munzimi et al.* [2014] and *Nicholson* [2000] draw similar conclusions.

223 The simulated monthly precipitation and temperature values were temporally
224 downscaled to daily values for use in the CRB hydrology model. We used the three-
225 hourly and monthly observed historical data developed for the Global Land Data
226 Assimilation System [*Rodell et al.*, 2004; *Sheffield et al.*, 2006] and the bias-corrected
227 monthly simulations to generate three-hourly precipitation and temperature fields, which
228 were subsequently aggregated to obtain daily values (see SI Methods). The hydrological
229 model was forced with the bias-corrected and downscaled daily climate fields for the
230 period 1950-2065. Due to the lack of information on the effect of CO₂ on the 16 land
231 cover classes simulated, the ambient CO₂ concentration was maintained at 330 ppm
232 throughout the simulation period. A recent study suggests that, in tropical rainforest
233 catchments, elevated CO₂ has little impact on evapotranspiration, but results in increased
234 plant assimilation and light use efficiency [*Yang et al.*, 2016]. A total of 50 projections
235 (25 RCP4.5 and 25 RCP8.5 projections) were compiled and analyzed. Results of
236 individual and multi-model means (un-weighted average of all (MM) and selected (SM)
237 GCM simulations) for the near-term (2016-2035) and mid-term (2046-2065) projections
238 are presented.

239 **3. Results and Discussion**

240 ***3.1 Historical simulations***

241 Historical observations of average annual precipitation vary from 1,100 mm in the
242 southeastern portion of the CRB to 1,600 mm in the CRB's equatorial region. We
243 compared the GCM-simulated annual precipitation and its inter-annual variability during
244 the historical period with observations from 30 locations within the CRB (Figure 2). The
245 simulated inter-annual variability among the climate models (vertical bars in Figure 2)
246 lies within the range of the observed variability (horizontal bars in Figure 2). The linear-
247 regression slope of 1.16 ($p < 0.001$, Figure 2) between the annual observed and the multi-
248 model mean shows that bias-corrected precipitation is slightly over-estimated, but not
249 significantly so. Observations of seasonal precipitation are reproduced similarly well by
250 the GCM models (SI Figure S2 and Table S2). The good agreement between GCM-
251 simulated and observed rainfall is expected given our bias correction of the GCM output.

252 We compared the simulated monthly runoff at 30 locations with observations
253 (Figure 3A). The colored points compare observed mean annual runoff at the 30 gage
254 locations with historical simulations (hydrological model forced with observed climate),
255 while the vertical and horizontal bars show the modeled and observed inter-annual
256 variability, respectively. The shades of colors (from light-green to yellow and red) reveal
257 the model's skill in simulating the monthly flows in the historical period. The Nash-
258 Sutcliffe coefficient of efficiency (NSE), a measure of relative magnitude of residual
259 variance compared to the monthly observed streamflow variance [*Legates and McCabe,*
260 *1999; Nash and Sutcliffe, 1970*], varies between 0.01 and 0.86 (color scale in Figure 3A).
261 (The NSE ranges between negative infinity to 1, with values between 0.5 and 1

262 considered satisfactory [*Moriasi et al.*, 2007].) Seventeen of the 30 gages show NSE
263 greater than or equal to 0.5. Higher NSE values at locations on both sides of the equator,
264 particularly at major tributaries (NSE ~ 0.60, gages 1 to 8 in Figure 1 and SI Figure S3)
265 suggest that the model reliably simulates stream flows under different climatic
266 conditions. High NSE values also indicate that the seasonal and annual runoff
267 simulations, including the inter-annual variability in the historical period, are in good
268 agreement with observations. The catchment areas of the 30 gages vary between 5,000
269 km² and 900,000 km² (excluding the last two downstream gages) and encompass a range
270 of land cover and climatic regions on both sides of the equator; thus the hydrology model
271 exhibits reasonable skill in simulating runoff over a wide range of watershed conditions.

272 Comparison of modeled runoff forced with GCM-simulated and observed climate
273 (Figure 3B) reveals generally acceptable runoff simulations in the CRB. The black dots
274 and red (blue) vertical bars in Figure 3B show multi-model mean and maximum
275 (minimum) range of inter-annual variability in the 25 historical GCM simulations. The
276 results suggest that model-data agreement in precipitation translates to similarly
277 acceptable runoff simulations.

278 Runoff patterns reflect seasonal rainfall that varies asymmetrically on either side
279 of the equator (see SI Figure S1). For example, the observed peak runoff at streamflow
280 gages 2 and 6 (see Figure 1) located north and south of the equator occur near the end of
281 the rainy seasons – during Sep-Oct and Mar-Apr, respectively (Figure 4). Augmented by
282 flows from northern and southern tributaries (e.g. gages 1, 2, 4 and 6) and by high
283 precipitation in the tropical equatorial watersheds during the two wet seasons (MAM and
284 SON), the main river flows (downstream of gage 3 in Figure 1) show low variability

285 (Figure 4). For example, the coefficient of variation in observed (simulated) monthly
286 flows at the basin outlet (gage 8), northern tributary (gage 2) and southern tributary (gage
287 4) are 0.23 (0.24), 0.77 (0.80) and 0.40 (0.48), respectively.

288 Regionally, runoff in the northern (NC) and southern (SW and SE) watersheds is
289 strongly seasonal with long dry seasons, but this is not the case in the equatorial region
290 (Figure 5). Average watershed runoff varies between 20-70 mm during dry seasons to
291 100-140 mm during wet seasons in the NC, SW and SE. In the equatorial region, seasonal
292 runoff varies between 100-150mm with the highest in SON. Overall, the precipitation-
293 runoff ratio is about 0.30 in the CRB. The accessible runoff (excluding runoff associated
294 with flood events), which can be appropriated for human use, is about 70% of the total
295 runoff.

296 ***3.2 Future projections in precipitation and runoff***

297 ***3.2.1 Precipitation***

298 A previous study [Aloysius *et al.*, 2016] showed that GCM projections of
299 temperature generally increase under both emission scenarios in line with historical
300 upward trend for Africa [Hulme, 2001]; however, precipitation projections contain large
301 uncertainties. The modeled near-term (2016-2035) precipitation projections in the CRB
302 vary between -4% and 6% with a multi-model mean (MM) change of 1% under the two
303 emission scenarios relative to the reference period (1986-2015). Regionally, the northern
304 CRB shows the largest annual increase in precipitation followed by southwestern and
305 equatorial regions. However, the inter-model variability is larger than the MM in all
306 regions, indicating greater projection uncertainties in both emission scenarios (Table 2).

307 The mid-term (2046-2065) projections of annual precipitation vary between -5% and 9%,
308 with the MM of 1.7% and 2.1% for RCP4.5 and RCP8.5, respectively. More than 70% of
309 the ensembles in both RCPs project an increase in annual precipitation in the CRB over
310 the mid-term. The multi-model mean of all ensembles that project an increase (decrease)
311 in precipitation is 2.7% (-2.4%) for RCP4.5 and 4.0% (-2.9%) for RCP8.5.

312 The GCMs project considerable spatial and seasonal variations in precipitation
313 (Table 2 and Figure 6). However, the standard deviation of annual and seasonal
314 projections within the four regions exceed or equal to the MM, indicating little agreement
315 on the direction of change. The spatial patterns (Figure 6), on the other hand, show
316 regions where modeled projections strongly agree on increasing or decreasing
317 precipitation. For example, decreasing precipitation is projected in most of the headwater
318 catchments in the southern and parts of northern CRB.

319 In general, the GCMs project decreasing precipitation in the driest parts of the
320 southern CRB (mostly in Southeastern CRB, but portions of Southwestern as well).
321 Under the RCP8.5 scenario, the northeastern CRB also experiences reduction in
322 precipitation in the near-term. The areas of decreased precipitation shrink in the southeast
323 and southwest in the mid-term; however, drying expands in parts of northern CRB under
324 the two emission scenarios. Most GCMs (14-20) project an increase in all but the
325 southeastern CRB.

326 Inter-model variability in precipitation projections are sensitive to seasons and
327 climate region (Figure 7A-D). At monthly scale, the northern and southern regions
328 receive less than 50mm of precipitation for at least three months, which persist in the
329 future under both emission scenarios. The dry season is more prolonged in the southeast

330 compared to the rest of the CRB. The inter-model variability is larger in the rainy seasons
331 under RCP8.5, compared to RCP4.5. Larger variability under RCP8.5 highlights that
332 GCMs may have limited skill in simulating precipitation under high greenhouse gas
333 emissions.

334 **3.2.2 Runoff**

335 In general, modeled runoff increases, and its inter-annual variability within GCMs
336 is larger during high flow periods compared to low flow periods, except in the equatorial
337 region (Figure 7E-H, see Figure 1 for regions). The model projection uncertainty
338 increases towards the middle of century, particularly under the RCP8.5 emission
339 scenario. The temporal patterns of runoff in the near- and mid-terms are similar to the
340 precipitation patterns, but with a time lag. As with precipitation, the monthly runoff
341 shows prolonged periods low values in the northern and southern CRB in both projection
342 periods. Spatially, parts of northern, southeastern, and southwestern CRB also show
343 reduced runoff projections relative to the reference period under both RCPs; these
344 reductions are predominantly in the areas where fewer GCMs agree on the increase in
345 modeled precipitation (see Figure 6 and SI Tables S3 and S4). The area of decreasing
346 runoff expands in the northern CRB under both emission scenarios in the mid-term (see
347 Figure 6, which shows that more models agree on decreasing precipitation in parts of
348 northern CRB that subsequently results in decreasing runoff). Although the northern and
349 equatorial CRB show an overall increase in precipitation, the decrease in runoff in certain
350 parts in the northern and equatorial CRB is caused by reduction in seasonal precipitation.
351 A larger reduction – up to 15% – in the southeastern CRB covering most of northern

352 Zambia is due to an overall decrease in precipitation simulated by more the half of the
353 GCMs (see Figure 6).

354 The multi-model mean of total runoff from the CRB shows an increase of 5%
355 ($\pm 6\%$, one standard deviation, $n = 25$) and 7% ($\pm 8\%$) in the near- and mid-terms under
356 both RCPs relative to the reference period (1986-2005). Annual Runoff in the equatorial
357 region, which receives the highest precipitation, is projected to increase by up to 5%
358 ($\pm 7\%$) in the near-term to 6% ($\pm 8\%$) and 7% ($\pm 9\%$) in the mid-term for RCP4.5 and
359 RCP8.5, respectively. The increases are greater in the secondary rainy season (MAM)
360 than the primary (SON, Figure 7 B and F). Monthly runoff projections show that the
361 majority of the ensembles project an increase in the equatorial CRB, with the RCP8.5
362 ensembles exhibiting larger variability (Figure 7F).

363 Runoff that can be appropriated for human use is generated mostly in the
364 northern, southeastern and southwestern CRB, which at present varies from 130mm/year
365 in the southeastern CRB to 250-400mm/year in the northeastern and southwestern CRB.
366 Runoff is projected to increase in all three of these regions. However, the inter-model
367 variability is greater than twice the MM in nearly all the regions and during all four
368 seasons (Figure 8 and Table 3). In most cases, the largest uncertainties are in non-rainy
369 seasons and under high emission RCP8.5 scenario (e.g. DJF in the northern CRB, Figure
370 8B, and JJA in the southeastern CRB, Figure 8H).

371 ***3.3 Variability in accessible flows***

372 Only part of the runoff may be appropriated for human use. In the CRB, the
373 **accessible runoff (AF)**, excluding runoff associated with flood events, is about 70%. The

374 AF is largely under-utilized, but its appropriation is expected to increase in the future,
375 mostly in the populated areas of northern, southwestern and southeastern CRB. We
376 present the uncertainty associated with GCM and scenario selection by quantifying
377 seasonal and inter-model variability in AF at eight major tributaries (identified in Figure
378 1) that drain watersheds across a range of climatic regions on both sides of the equator
379 (Figure 9). Modeled AF exhibits substantial inter-model spread in the near-term and
380 widens in the mid-term (SI Figure S5). The inter-model variability is larger during high
381 flow periods compared to low flow periods.

382 Following the general pattern of increasing precipitation and runoff in the
383 northern and southwestern watersheds, we find that AF increases with greater model
384 agreement in tributaries that drain these watersheds (e.g. gages 1, 2 and 6 in Figure 9). A
385 closer look at tributaries in the northern and southwestern CRB reveals better agreement
386 of increased AF during low flow periods compared to high flow periods (compare gages
387 1, 2, 6 and 7 in Figure 9). In contrast, tributaries that drain southeastern watersheds
388 exhibit greater variability in modeled AF with majority of the ensembles projecting a
389 reduction (e.g. gages 4 and 5 in Figure 7). Overall, the AF in the main tributary (gages 3
390 and 8) is projected to increase, partly due to the contributions from the northern and
391 southwestern tributaries. The decrease in modeled precipitation and AF in the
392 southeastern CRB appears to have marginal effect on downstream flows in the main
393 river.

394 The spatial and temporal variations in the projected AF have consequences for
395 water resources development and management. For example, the uncertainty in
396 projections of the AF near the proposed Grand Inga Hydropower project (near gage 8,

397 *Showers* [2009]) is low compared the projections near the proposed trans boundary water
398 diversion in the southeast (near gage 5, *Lund et al.* [2007]). Reductions in high and low
399 flows in streams in the southeastern region will have implications to aquatic life, channel
400 maintenance and lake and wetland flooding.

401 ***3.4 Sources of uncertainty***

402 Climate model outputs under the two emission scenarios used in this study
403 provide an opportunity to assess a range of future projections that could potentially
404 resolve wide variations in results and, hence, uncertainties in modelled projections for the
405 CRB. The uncertainties can be broadly categorized into i) observational uncertainty,
406 particularly the sparse and declining network of precipitation and stream flow gages and
407 ii) model uncertainty, which, in GCMs, include model structure, model initialization,
408 parameterization and climate sensitivity – the response of global temperature to a
409 doubling of CO₂ in the atmosphere relative to pre-industrial levels. We used only one
410 hydrological model, which is also a source of uncertainty. However, variation in climate
411 signals between GCMs and emissions scenarios, particularly precipitation projections,
412 may be a larger source of uncertainty than the choice of hydrology model [*Thompson et*
413 *al.*, 2014; *Vetter et al.*, 2016].

414 The climate data used for bias-correction and for historical hydrologic simulations
415 has its own uncertainties. Gage-based, satellite derived data and reanalysis outputs are
416 used to develop the historical observations [*Sheffield et al.*, 2006]. Precipitation gages
417 were more numerous at the beginning of the simulation period and declined in number
418 toward the end of the 20th century [*Mitchell and Jones*, 2005; *Washington et al.*, 2013].
419 Available gage data varied both spatially and temporally (SI Figure S6 and S7). For

420 example, the equatorial region – nearly a third of CRB – had about 70 rain gages through
421 early 1990s, but only 10% of these were functioning by 2005 (SI Figure S5). The
422 southeastern and parts of northern CRB also had good rainfall-gage coverage, which has
423 similarly decreased since the 1990s [*Mitchell and Jones, 2005*]. However, satellite-based
424 and sparsely distributed gage data has been used to demonstrate that spatiotemporal
425 distribution of precipitation can be sufficiently described in the CRB region [*Munzimi et*
426 *al., 2014; Nicholson, 2000; Samba et al., 2008*]. We assume that, even with these
427 limitations, the available historical data are adequate to model the hydrology of the CRB.

428 In addition to climate data, observed runoff data are another limitation that could
429 restrict proper validation of hydrological models. However, we utilized a time period
430 (1950-1959) when the CRB had maximum coverage of both precipitation and runoff data
431 to calibrate and validate the hydrology model (for example see evidence in *L'vovich*
432 [*1979*]). Where available, we used additional runoff data to further validate model
433 outputs in the historical period. The runoff gage locations are distributed within the CRB
434 (see Figure 1) such that they adequately capture climatic, land cover and topographic
435 variability.

436 For future projections, the largest sources of uncertainty arise from the GCMs and
437 emission scenarios. GCMs do not consistently capture observed rainfall seasonality and
438 heavy rainfall in regions of the central CRB, and in most cases do not show key features
439 such as seasonality and heavy rainfall regions of central CRB [*Aloysius et al., 2016;*
440 *Washington et al., 2013*]. The biases in the GCM-simulated precipitation, particularly in
441 the tropical regions, have been attributed to multiple factors including poorly resolved
442 physical processes such as the mesoscale convection systems, inadequately resolved

443 topography due to the coarse horizontal resolution and inadequate observations to
444 constrain parameterization schemes. These limitations are unavoidable in the current set
445 CMIP5 projections. We assume that the number of GCM outputs used in our work, and
446 the bias-correction method, which maintains key statistical properties in the original
447 GCM outputs (see *Aloysius et al.* [2016] and *Li et al.* [2010]), adequately captures the
448 uncertainties in GCM and emission scenarios. Based on monthly precipitation
449 climatology, *Aloysius et al.* [2016] found no significant shift in seasonality in modeled
450 future precipitation projections.

451 The range of projections presented here for the two emission scenarios also
452 highlight the uncertainties planners would encounter when making climate-related
453 decisions. For example, broader agreement on increase in runoff in parts of the CRB
454 would help make robust decisions, whereas weaker agreement in the southern CRB calls
455 for greater scrutiny of regional climate. Generally, the MM approach reduces the
456 uncertainty because averaging tend to offset errors across models. However, one could
457 also ask whether this approach work with fewer models.

458 *Washington et al.* [2013] and *Siam et al.* [2013] presented evidence that
459 evaluating atmospheric moisture flux which are modulated by wind patterns and
460 humidity, and soil water balance are better ways to diagnose GCM performance in data
461 scarce regions like the CRB. *Balas et al.* [2007], *Hirst and Hastenrath* [1983] and
462 *Nicholson and Dezfuli* [2013] have shown that sea surface temperature (SST) anomalies
463 in the Atlantic and Indian ocean sectors could partly explain precipitation in the CRB
464 region. Along the same lines, *Aloysius et al.* [2016] identified five models as suitable
465 candidates. We examined this subset of GCM projections (M6, M7, M18, M23 and

466 M24), which we refer to as the select model average, or SM (see refs. *Giorgetta et al.*
467 [2013]; *Good et al.* [2012]; *Jungclaus et al.* [2013]; *Meehl et al.* [2013]; *Siam et al.*
468 [2013]; *Voldoire et al.* [2012]; *Yukimoto et al.* [2006] and *Aloysius et al.* [2016] for
469 further comparison of GCM performance). By evaluating seasonal atmospheric moisture
470 and soil water balance in 11 CMIP5 GCMs in the CRB and Nile River basin regions,
471 *Siam et al.* [2013] identified M7, M18 and M24 as good candidates for climate change
472 assessment.

473 Focusing on the northern, southeastern and southwestern CRB, where human
474 appropriation of runoff is expected to increase, we find that the magnitude of annual
475 projections (both precipitation and runoff) in SM are more than twice that of MM in the
476 northern region. The extent of drying in the south is concentrated in the southeastern
477 upstream watersheds in both MM and SM, although the magnitude of decrease is smaller
478 in SM (SI Table S3 and S4).

479 From the viewpoint of water resources for human appropriation, the changes by
480 seasons are also important. Future changes and uncertainties in modeled seasonal runoff
481 averaged over the four regions are presented Figure 8. In comparison with the CRB
482 projections, the uncertainties in sub-regions are larger. Nearly all the MM and SM
483 projections show an increase in runoff in all the four seasons; however, there is
484 substantial inter-model variability. The uncertainties increase under the high emission
485 RCP8.5 scenario during the mid-century. Considering the southeastern region as an
486 example, under RCP8.5 emission scenario, uncertainties reported as one inter-model
487 standard deviation in the mid-term are $\pm 20\%$, $\pm 27\%$, $\pm 26\%$ and $\pm 13\%$, respectively for
488 DJF, MAM, JJA and SON seasons, and are greater than the MM and SM. Further, the

489 deviation of uncertainty within the sub-regions of CRB increases under high emission
490 RCP8.5 scenario. For example, the inter-model projection ranges are larger in the
491 northern and southeastern CRB (Figure 8 B and H) compared to the equatorial and
492 southwestern CRB (Figure 8 D and F). Finally, the uncertainty assessment presented here
493 represents climate model uncertainty arising from emission scenarios, different response
494 to the same external forcing, different model structures and parameterization schemes.
495 While these uncertainties in projections pose challenges for robust decision making, they
496 also provide insights into where further research might be most valuable.

497 **4. Conclusions**

498 From the point of view of climate change adaptation related to water resources,
499 agriculture, and ecosystem management, the challenge faced by CRB countries is
500 recognizing the value of making timely decisions in the absence of complete knowledge.
501 In some settings, climate change presents opportunities as well as threats in the CRB. The
502 projected increases in accessible runoff imply new opportunities to meet increasing
503 demands (e.g. drinking water, food production and sanitation), while the enhanced flood
504 runoff would pose new challenges (e.g. flood protection and erosion control). On the
505 other hand, water managers could face different challenges in the southeast where
506 precipitation and runoff are projected to decrease.

507 GCM-related variability in regional climate projections could be constrained by a
508 subset of models based on attributes that modulate large-scale circulations (see *Knutti*
509 *and Sedlacek* [2013] and *Masson and Knutti* [2011]). This approach is particularly useful
510 because regions like the CRB lack complete coverage of observational data but the
511 mechanisms that moderate the climate system, particularly precipitation, are fairly well

512 understood [*Hastenrath, 1984; Nicholson and Grist, 2003; Washington et al., 2013*]. Yet,
513 the span in rainfall predictions among the MM, SM, and individual GCMs suggest that,
514 despite the advances in climate modeling, significant uncertainties in precipitation
515 projections for CRB persist.

516 Rather than providing a narrow pathway for decision-making, our results, for the
517 first time for CRB, provide a framework to i) assess implications under various climate
518 model assumptions and uncertainties, ii) characterize and expose vulnerabilities and iii)
519 provide ways to guide the search for impact-oriented and actionable policy alternatives,
520 as emphasized by *Weaver et al. [2013]*. Projections and associated uncertainties vary
521 widely by region within the CRB, and therefore diverse but robust planning strategies
522 might be advisable within the river basin. We emphasize that projections provided here
523 could be considered as part of the process of incorporating multiple stressors into climate
524 change adaptation and engaging stakeholders in the decision making process.

525 **Acknowledgements**

526 We would like to thank Nadine Laporte, Innocent Liengola, Peter Umunay, Greg Fiske
527 and Melanie Burr for help with data and literature search. We acknowledge the World
528 Climate Research Program's Working Group on Coupled Modeling, which is responsible
529 for CMIP, and we thank the climate modeling groups (Table 1) for producing and making
530 available their model output. For CMIP, the U.S. Department of Energy's Program for
531 Climate Model Diagnosis and Inter-comparison provides coordinating support and led
532 development of software infrastructure in partnership with the Global Organization for
533 Earth System Science Portals. We gratefully acknowledge the efforts of two anonymous
534 reviewers who made thoughtful comments that substantially improved the manuscript.

535 This work was supported in part by the facilities and staff of the Yale University Faculty
536 of Arts and Sciences High Performance Computing Center, and by the National Science
537 Foundation under grant CNS 08-21132 that partially funded acquisition of the facilities.
538

539 **References**

- 540 Adams, W. M., A. Goudie, and A. R. Orme (1996), *The physical geography of Africa*,
541 Oxford University Press, Oxford, New York.
- 542 Aloysius, N., J. Sheffield, J. E. Sainers, H. Li, and E. F. Wood (2016), Evaluation of
543 historical and future simulations of precipitation and temperature in Central Africa from
544 CMIP5 climate models, *Journal of Geophysical Research - Atmospheres*, 121(1), 130-
545 152.
- 546 Alsdorf, D., E. Beighley, A. Laraque, H. Lee, R. Tshimanga, F. O'Loughlin, G. Mahé, B.
547 Dinga, G. Moukandi, and R. G. M. Spencer (2016), Opportunities for hydrologic research
548 in the Congo Basin, *Reviews of Geophysics*, 54(2), 378-409.
- 549 Arnold, J. G., R. Srinivasan, R. S. Muttiah, and J. R. Williams (1998), Large area
550 hydrologic modeling and assessment part I: Model development, *Journal of the American*
551 *Water Resources Association*, 34(1), 73-89.
- 552 Balas, N., S. E. Nicholson, and D. Klotter (2007), The relationship of rainfall variability
553 in West Central Africa to sea-surface temperature fluctuations, *International Journal of*
554 *Climatology*, 27(10), 1335-1349.
- 555 Bartholomé, E., and A. S. Belward (2005), GLC2000: A new approach to global land
556 cover mapping from Earth observation data, *International Journal of Remote Sensing*,
557 26(9), 1959-1977.
- 558 Beighley, R. E., R. L. Ray, Y. He, H. Lee, L. Schaller, K. M. Andreadis, M. Durand, D.
559 E. Alsdorf, and C. K. Shum (2011), Comparing satellite derived precipitation datasets
560 using the Hillslope River Routing (HRR) model in the Congo River Basin, *Hydrological*
561 *Processes*, 25(20), 3216-3229.
- 562 Bruinsma, J. (2003), *World agriculture: towards 2015/2030: An FAO perspective*, 520
563 pp., Earthscan/James & James, London, UK.
- 564 Bultot, F., and J. F. Griffiths (1972), The Equatorial Wet Zone, in *Climate of Africa*,
565 edited by J. F. Griffiths, pp. 259-291, Elsevier Publishing Company, Amsterdam.
- 566 Burney, J. A., R. L. Naylor, and S. L. Postel (2013), The case for distributed irrigation as
567 a development priority in sub-Saharan Africa, *Proceedings of the National Academy of*
568 *Sciences*, 110(31), 12513-12517.
- 569 Center for International Earth Science Information Network (CIESIN) Columbia
570 University, United Nations Food and Agriculture Programme (FAO), and C. I. d. A. T.
571 (CIAT) (2005), *Gridded Population of the World: Future Estimates (GPWFE)*, edited,
572 Center for International Earth Science Information Network (CIESIN) Columbia
573 University, New York, United States.
- 574 Collier, P., G. Conway, and T. Venables (2008), Climate change and Africa, *Oxford*
575 *Review of Economic Policy*, 24(2), 337-353.
- 576 DeFries, R., and C. Rosenzweig (2010), Toward a whole-landscape approach for
577 sustainable land use in the tropics, *Proceedings of the National Academy of Sciences*,
578 107(46), 19627-19632.

579 Doherty, J. (2004), *PEST: Model-independent Parameter Estimation, User Manual Fifth*
580 *Edition*, Watermark Numerical Computing, Brisbane, Australia.

581 FAO/IIASA (2009), Harmonized World Soil Database (version 1.1), in *Food and*
582 *Agricultural Organization and IIASA*, edited, Rome, Italy and Laxenburg, Austria.

583 Faramarzi, M., K. C. Abbaspour, S. Ashraf Vaghefi, M. R. Farzaneh, A. J. B. Zehnder, R.
584 Srinivasan, and H. Yang (2013), Modeling impacts of climate change on freshwater
585 availability in Africa, *Journal of Hydrology*, 480(0), 85-101.

586 Gibbs, H. K., A. S. Ruesch, F. Achard, M. K. Clayton, P. Holmgren, N. Ramankutty, and
587 J. A. Foley (2010), Tropical forests were the primary sources of new agricultural land in
588 the 1980s and 1990s, *Proceedings of the National Academy of Sciences*, 107(38), 16732-
589 16737.

590 Giorgetta, M. A., et al. (2013), Climate and carbon cycle changes from 1850 to 2100 in
591 MPI-ESM simulations for the coupled model intercomparison project phase 5, *Journal of*
592 *Advances in Modeling Earth Systems*, 5(3), 572-597.

593 Global Runoff Data Center. (2011), Long-Term Mean Monthly Discharges and Annual
594 Characteristics of GRDC Stations, edited by G. R. D. Center., Federal Institute of
595 Hydrology, Koblenz, Germany.

596 Good, P., C. Jones, J. Lowe, R. Betts, and N. Gedney (2012), Comparing tropical forest
597 projections from two generations of Hadley Centre Earth System models, HadGEM2-ES
598 and HadCM3LC, *Journal of Climate*, in press.

599 Hansen, M. C., D. P. Roy, E. Lindquist, B. Adusei, C. O. Justice, and A. Altstatt (2008),
600 A method for integrating MODIS and Landsat data for systematic monitoring of forest
601 cover and change in the Congo Basin, *Remote Sensing of Environment*, 112(5), 2495-
602 2513.

603 Hastenrath, S. (1984), Interannual variability and annual cycle: Mechanisms of
604 circulation and climate in the tropical Atlantic sector, *Monthly Weather Review*, 112(6),
605 1097-1107.

606 Hirst, A. C., and S. Hastenrath (1983), Diagnostics of hydrometeorological anomalies in
607 the Zaire (Congo) basin, *Quarterly Journal of the Royal Meteorological Society*,
608 109(462), 881-892.

609 Hulme, M., Doherty, R., Ngara, T., New, M., and Lister, D. (2001), African Climate
610 Change: 1900-2100, *Climate Research*, 17, 145-168.

611 IPCC (2014), Summary for policymakers. In: *Climate Change 2014: Impacts,*
612 *Adaptation, and Vulnerability. Part A: Global and Sectoral Aspects. Contribution of*
613 *Working Group II to the Fifth Assessment Report of the Intergovernmental Panel on*
614 *Climate Change Rep.*, 1-32 pp, Intergovernmental Panel on Climate Change, Cambridge,
615 UK.

616 Jungclauss, J. H., N. Fischer, H. Haak, K. Lohmann, J. Marotzke, D. Matei, U.
617 Mikolajewicz, D. Notz, and J. S. von Storch (2013), Characteristics of the ocean
618 simulations in the Max Planck Institute Ocean Model (MPIOM) the ocean component of

619 the MPI-Earth system model, *Journal of Advances in Modeling Earth Systems*, 5(2), 422-
620 446.

621 Knutti, and J. Sedlacek (2013), Robustness and uncertainties in the new CMIP5 climate
622 model projections, *Nat Clim Change*, 3, 369–373.

623 Krysanova, V., and M. White (2015), Advances in water resources assessment with
624 SWAT—an overview, *Hydrological Sciences Journal*, 60(5), 771-783.

625 L'vovich, M. I. (1979), *World water resources and their future*, American Geophysical
626 Union.

627 Laporte, N. T., S. J. Goetz, C. O. Justice, and M. Heinicke (1998), A new land cover map
628 of central Africa derived from multi-resolution, multi-temporal AVHRR data,
629 *International Journal of Remote Sensing*, 19(18), 3537-3550.

630 Lee, H., R. E. Beighley, D. Alsdorf, H. C. Jung, C. K. Shum, J. Duan, J. Guo, D.
631 Yamazaki, and K. Andreadis (2011), Characterization of terrestrial water dynamics in the
632 Congo Basin using GRACE and satellite radar altimetry, *Remote Sensing of*
633 *Environment*, 115(12), 3530-3538.

634 Legates, D. R., and G. J. McCabe, Jr. (1999), Evaluating the use of "Goodness-of-Fit"
635 measures in hydrologic and hydroclimatic model validation, *Water Resour. Res.*, 35(1),
636 233-241.

637 Lehner, K. Verdin, and A. Jarvis (2008), New Global Hydrography Derived from
638 Spaceborne Elevation Data, *Eos. Trans. AGU*, 89(10).

639 Lempicka, M. (1971), Bilan hydrique du bassin du fleuve Zaire. *Rep.*, Office National de
640 la Recherche et du Development, Kinshasa, DRC.

641 Li , H., J. Sheffield, and E. F. Wood (2010), Bias correction of monthly precipitation and
642 temperature fields from Intergovernmental Panel on Climate Change AR4 models using
643 equidistant quantile matching, *Journal of Geophysical Research - Atmospheres*,
644 115(D10), D10101.

645 Lund, B., E. Snell, D. Easton, and A. De Beer (2007), Aqueduct to link Central Africa
646 with Southern Africa? A brief outline, *Civil Engineering = Siviele Ingenieurswese*,
647 15(10), 4-8.

648 Malhi, Y., and J. Grace (2000), Tropical forests and atmospheric carbon dioxide, *Trends*
649 *in Ecology & Evolution*, 15(8), 332-337.

650 Masson, D., and R. Knutti (2011), Climate model genealogy, *Geophysical Research*
651 *Letters*, 38(8), L08703.

652 Matungulu, K.-M. (1992), Characterization and fertility evaluation of some major soil
653 groups from Zaire (Central Africa), North Carolina State University, Raleigh, North
654 Carolina.

655 Meehl, G. A., W. M. Washington, J. M. Arblaster, A. Hu, H. Teng, J. E. Kay, A.
656 Gettelman, D. M. Lawrence, B. M. Sanderson, and W. G. Strand (2013), Climate change
657 projections in CESM1(CAM5) compared to CCSM4, *Journal of Climate*, 26(17), 6287-
658 6308.

- 659 Mitchell, T. D., and P. D. Jones (2005), An improved method of constructing a database
660 of monthly climate observations and associated high-resolution grids, *International*
661 *Journal of Climatology*, 25(6), 693-712.
- 662 Molden, D. (Ed.) (2007), *Water for food, water for life : A comprehensive assessment of*
663 *water management in agriculture*, 645 pp., Earthscan and International Water
664 Management Institute, London, UK and Colombo, Sri Lanka.
- 665 Moriasi, D. N., J. G. Arnold, M. W. Van Liew, R. L. Bingner, R. D. Harmel, and T. L.
666 Veith (2007), Model evaluation guidelines for systematic quantification of accuracy in
667 watershed simulations, *Transactions of the ASABE*, 50(3), 885-900.
- 668 Moss, R. H., et al. (2010), The next generation of scenarios for climate change research
669 and assessment, *Nature*, 463(7282), 747-756.
- 670 Munzimi, Y. A., M. C. Hansen, B. Adusei, and G. B. Senay (2014), Characterizing
671 Congo Basin Rainfall and Climate Using Tropical Rainfall Measuring Mission (TRMM)
672 Satellite Data and Limited Rain Gauge Ground Observations, *Journal of Applied*
673 *Meteorology and Climatology*, 54(3), 541-555.
- 674 Nash, J. E., and J. V. Sutcliffe (1970), River flow forecasting through conceptual models,
675 Part I. A discussion of principles, *Journal of Hydrology*, 10(3), 282-290.
- 676 Nathan, R. J., and T. A. McMahon (1990), Evaluation of automated techniques for base
677 flow and recession analyses, *Water Resources Research*, 26(7), 1465-1473.
- 678 Neitsch, S. L., J. G. Arnold, J. R. Kiniry, and J. R. Williams (2011), Soil Water
679 Assessment Tool - Theoretical Documentation - Version 2009Rep. 406, 647 pp, Texas
680 Water Resources Institute, Texas A&M University, Temple, Texas.
- 681 Niang, I., O. C. Ruppel, M. A. Abdrabo, A. Essel, C. Lennard, J. Padgham, and P.
682 Urquhart (2014), Africa, in *Climate Change 2014: Impacts, Adaptation, and*
683 *Vulnerability. Part B: Regional Aspects. Contribution of Working Group II to the Fifth*
684 *Assessment Report of the Intergovernmental Panel of Climate Change*, edited by V. R.
685 Barros, et al., pp. 1-115, Cambridge University Press, Cambridge, United Kingdom and
686 New York, NY, USA.
- 687 Nicholson, S. E. (2000), The nature of rainfall variability over Africa on time scales of
688 decades to millenia, *Global and Planetary Change*, 26(1-3), 137-158.
- 689 Nicholson, S. E., and J. P. Grist (2003), The seasonal evolution of the atmospheric
690 circulation over West Africa and Equatorial Africa, *Journal of Climate*, 16(7), 1013-
691 1030.
- 692 Nicholson, S. E., and A. K. Dezfuli (2013), The Relationship of Rainfall Variability in
693 Western Equatorial Africa to the Tropical Oceans and Atmospheric Circulation. Part I:
694 The Boreal Spring, *Journal of Climate*, 26(1), 45-65.
- 695 Nilsson, C., C. A. Reidy, M. Dynesius, and C. Revenga (2005), Fragmentation and Flow
696 Regulation of the World's Large River Systems, *Science*, 308(5720), 405-408.
- 697 Randall, D. A., et al. (2007), Climate Models and Their Evaluation, in *Climate Change*
698 *2007: The Physical Science Basis. Contribution of Working Group I to the Fourth*
699 *Assessment Report of the Intergovernmental Panel on Climate Change*, edited by S.

700 Solomon, D. Qin, M. Manning, Z. Chen, M. Marquis, K. B. Averyt, M. Tignor and H. L.
701 Miller, Cambridge University Press, Cambridge, United Kingdom and New York, NY,
702 USA.

703 Rodell, M., et al. (2004), The global land data assimilation system, *Bulletin of the*
704 *American Meteorological Society*, 85(3), 381-394.

705 Runge, J. (2007), The Congo River, Central Africa, in *Large Rivers: Geomorphology and*
706 *Management*, edited by A. Gupta, pp. 293-309, John Wiley, Chichester, England.

707 Salathé Jr, E. P., P. W. Mote, and M. W. Wiley (2007), Review of scenario selection and
708 downscaling methods for the assessment of climate change impacts on hydrology in the
709 United States pacific northwest, *International Journal of Climatology*, 27(12), 1611-
710 1621.

711 Samba, G., D. Nganga, and M. Mpounza (2008), Rainfall and temperature variations over
712 Congo-Brazzaville between 1950 and 1998, *Theoretical and Applied Climatology*, 91(1-
713 4), 85-97.

714 Schuol, J., K. C. Abbaspour, H. Yang, R. Srinivasan, and A. J. B. Zehnder (2008),
715 Modeling blue and green water availability in Africa, *Water Resources Research*, 44,
716 W07406.

717 Sheffield, J., G. Goteti, and E. F. Wood (2006), Development of a 50-year high-
718 resolution global dataset of meteorological forcings for land surface modeling, *Journal of*
719 *Climate*, 19(13), 3088-3111.

720 Showers, K. (2009), Congo River's Grand Inga hydroelectricity scheme: Linking
721 environmental history, policy and impact, *Water Hist*, 1(1), 31-58.

722 Siam, M. S., M.-E. Demory, and E. A. B. Eltahir (2013), Hydrological cycles over the
723 Congo and Upper Blue Nile Basins: Evaluation of general circulation model simulations
724 and reanalysis products, *Journal of Climate*, 26(22), 8881-8894.

725 Taylor, R. Stouffer, and G. Meehl (2012), An overview of CMIP5 and the experiment
726 design, *Bulletin of the American Meteorological Society*, 93(4), 485.

727 Teutschbein, C., and J. Seibert (2012), Bias correction of regional climate model
728 simulations for hydrological climate-change impact studies: Review and evaluation of
729 different methods, *Journal of Hydrology*, 456–457(0), 12-29.

730 Thompson, J. R., A. J. Green, and D. G. Kingston (2014), Potential evapotranspiration-
731 related uncertainty in climate change impacts on river flow: an assessment for the
732 Mekong River Basin, *Journal of Hydrology*, 510, 259-279.

733 Trambauer, P., S. Maskey, H. Winsemius, M. Werner, and S. Uhlenbrook (2013), A
734 review of continental scale hydrological models and their suitability for drought
735 forecasting in (sub-Saharan) Africa, *Physics and Chemistry of the Earth, Parts A/B/C*,
736 66(0), 16-26.

737 Tshimanga, R. M., and D. A. Hughes (2012), Climate change and impacts on the
738 hydrology of the Congo Basin: The case of the northern sub-basins of the Oubangui and
739 Sangha Rivers, *Physics and Chemistry of the Earth, Parts A/B/C*, 50–52(0), 72-83.

740 Tshimanga, R. M., and D. A. Hughes (2014), Basin-scale performance of a
741 semidistributed rainfall-runoff model for hydrological predictions and water resources
742 assessment of large rivers: The Congo River, *Water Resources Research*, 50(2), 1174-
743 1188.

744 UNEP (2011), *Water Issues in the Democratic Republic of the Congo: Challenges and*
745 *Opportunities Rep.*, United Nations Environment Program, Nairobi, Kenya.

746 van Griensven, A., P. Ndomba, S. Yalew, and F. Kilonzo (2012), Critical review of
747 SWAT applications in the upper Nile basin countries, *Hydrology and Earth System*
748 *Sciences*, 16(9), 3371-3381.

749 Vetter, T., et al. (2016), Evaluation of sources of uncertainty in projected hydrological
750 changes under climate change in 12 large-scale river basins, *Climatic Change*, 1-15.

751 Voltaire, A., et al. (2012), The CNRM-CM5.1 global climate model: Description and
752 basic evaluation, *Climate Dynamics*, 1-31.

753 Vorosmarty, C. J., B. M. Fekete, and B. A. Tucker (1998), Global River Discharge, 1807-
754 1991, Version 1.1 (RivDIS). Data set. Available on-line [<http://www.daac.ornl.gov>] from
755 Oak Ridge National Laboratory Distributed Active Archive Center, edited, Oak Ridge,
756 Tennessee, USA.

757 Washington, R., R. James, H. Pearce, W. M. Pokam, and W. Moufouma-Okia (2013),
758 Congo Basin rainfall climatology: Can we believe the climate models?, *Philosophical*
759 *Transactions of the Royal Society B: Biological Sciences*, 368(1625).

760 Weaver, C. P., R. J. Lempert, C. Brown, J. A. Hall, D. Revell, and D. Sarewitz (2013),
761 Improving the contribution of climate model information to decision making: the value
762 and demands of robust decision frameworks, *Wires Clim Change*, 4(1), 39-60.

763 Wohl, E., et al. (2012), The hydrology of the humid tropics, *Nat Clim Change*, 2(9), 655-
764 662.

765 Wood, A. W., L. R. Leung, V. Sridhar, and D. P. Lettenmaier (2004), Hydrologic
766 implications of dynamical and statistical approaches to downscaling climate model
767 outputs, *Climatic Change*, 62(1), 189-216.

768 World Bank Group (2014), *World Development Indicators*, edited, p. accessed May
769 2014, World Bank Publications.

770 World Food Program (2014), *Democratic Republic of Congo Rep.*, 113 pp, World Food
771 Program, Rome, Italy.

772 Yang, Y., R. J. Donohue, T. R. McVicar, M. L. Roderick, and H. E. Beck (2016), Long-
773 term CO2 fertilization increases vegetation productivity and has little effect on
774 hydrological partitioning in tropical rainforests, *Journal of Geophysical Research:*
775 *Biogeosciences*, 121(8), 2125-2140.

776 Yukimoto, S., A. Noda, A. Kitoh, M. Hosaka, H. Yoshimura, T. Uchiyama, K. Shibata,
777 O. Arakawa, and S. Kusunoki (2006), Present-day climate and climate sensitivity in the
778 Meteorological Research Institute coupled GCM version 2.3 (MRI-CGCM2. 3), *Journal*
779 *of the Meteorological Society of Japan*, 84(2), 333-363.

1 **Simulated Hydrologic Response to Projected Changes in Precipitation and Temperature in the Congo**
2 **River Basin**

3

4 Noel Aloysius^{1,2} and James Saiers¹

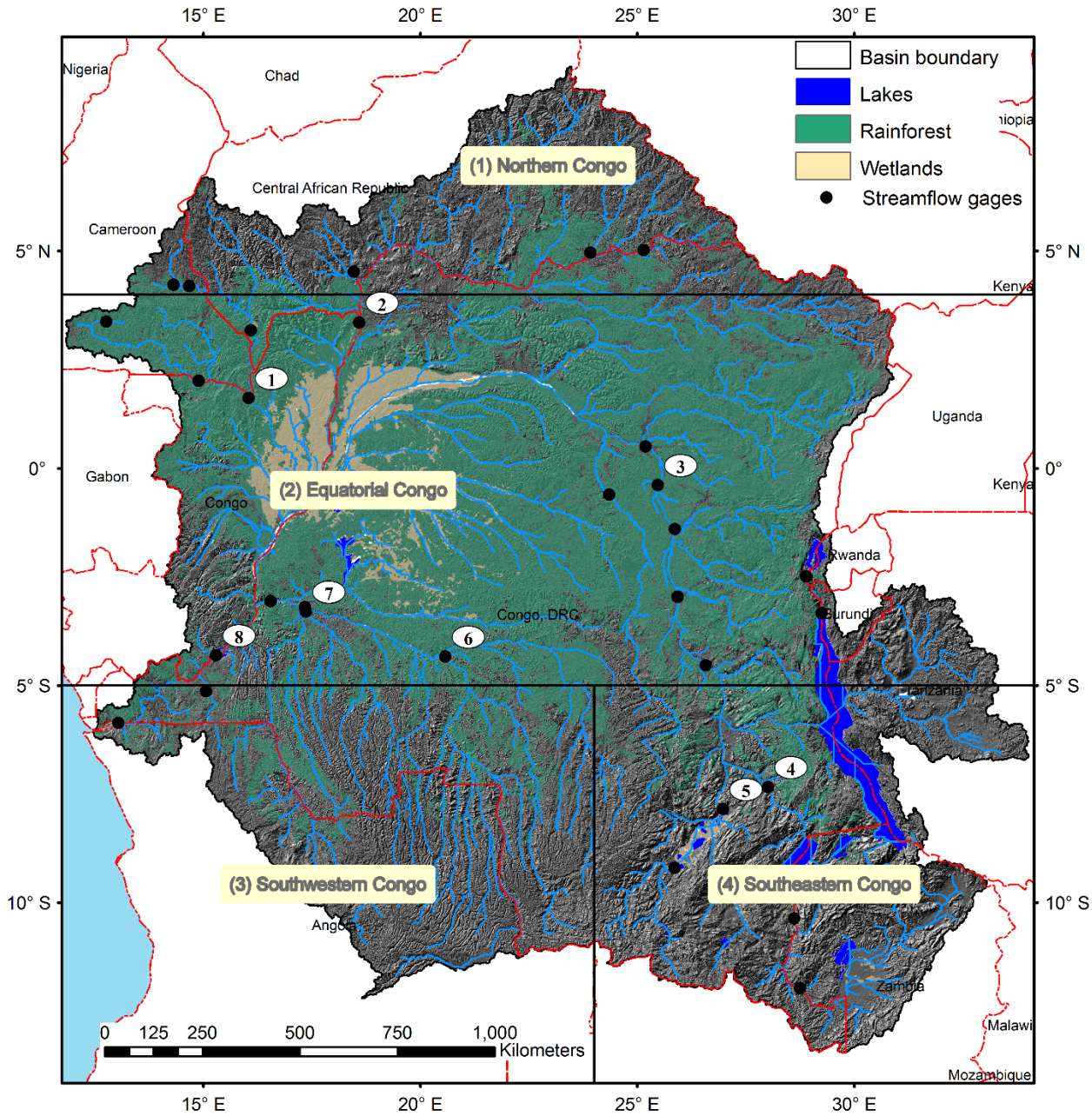
5 ¹ School of Forestry and Environmental Studies, Yale University, New Haven, Connecticut, USA

6 ² now at Department of Food, Agriculture & Biological Engineering and

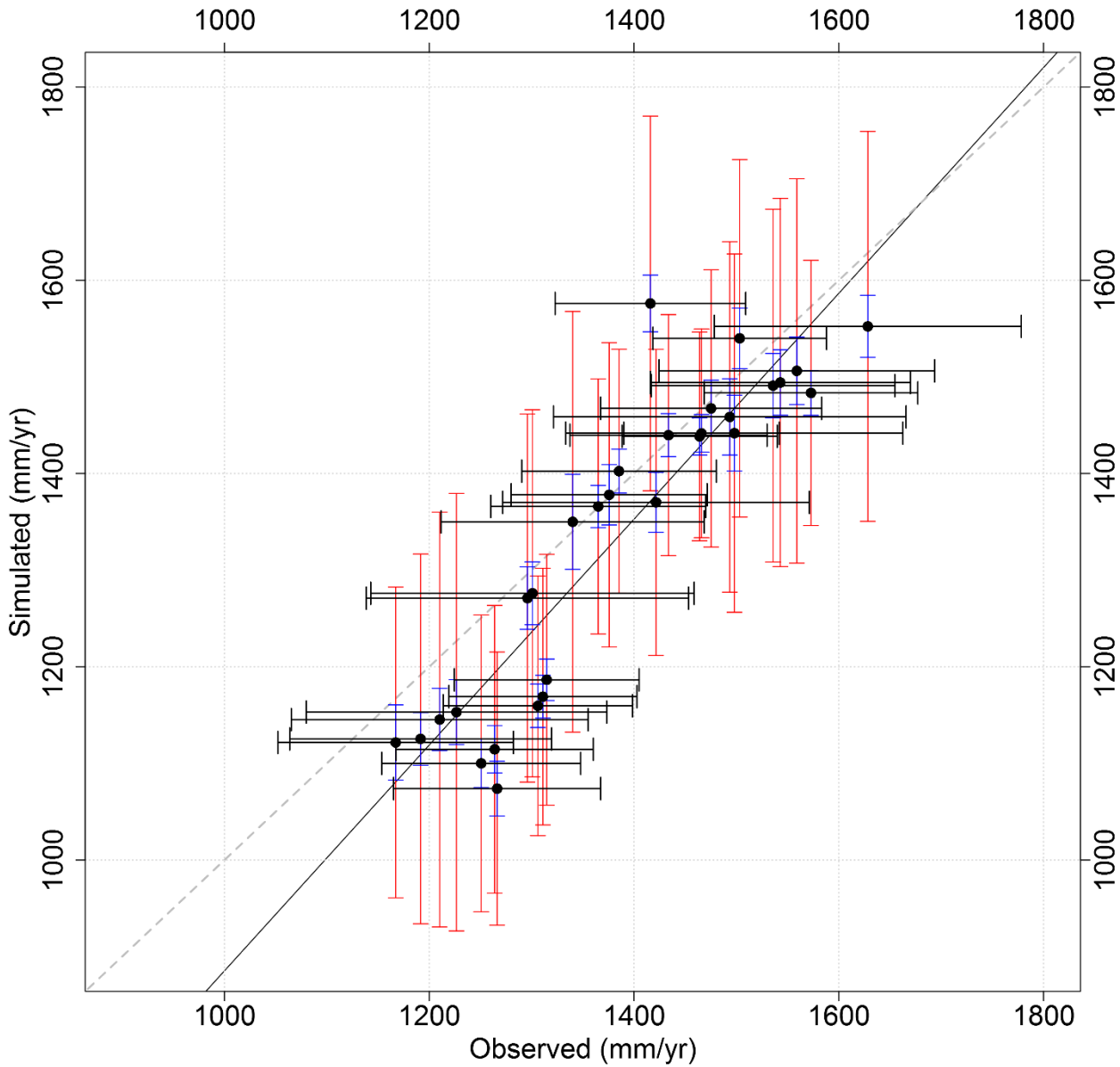
7 Aquatic Ecology Laboratory, Department of Evolution, Ecology and Organismal Biology

8 Ohio State University, Columbus, Ohio, USA

9



13 **Figure 1** Congo River Basin: the river basin boundary, the extent of the rainforest, locations of lakes and wetlands, and the
14 locations of streamflow gages are shown.



15

16 Figure 2 Comparison of observed and bias-corrected GCM-simulated average annual precipitation for 30 catchments with
 17 stream-flow gages (shown in Figure 1) in the historical period (1950-2005). Y-axis values are statistically downscales
 18 GCM-simulated precipitation. Black dots compare multi-model means with observed precipitation, black horizontal bars
 19 show observed inter-annual variability (\pm one standard deviation), and red (blue) vertical bars show maximum (minimum)
 20 range of modeled inter-annual variability (\pm one standard deviation) within the 25 climate model outputs. The black line is
 21 linear regression fit between observed and multi-model mean of simulated precipitation ($y = 1.16 \pm 0.204x -$
 22 $283.4, p < 0.001, R^2 = 0.825$); parameter bounds are 95% confidence interval.

23

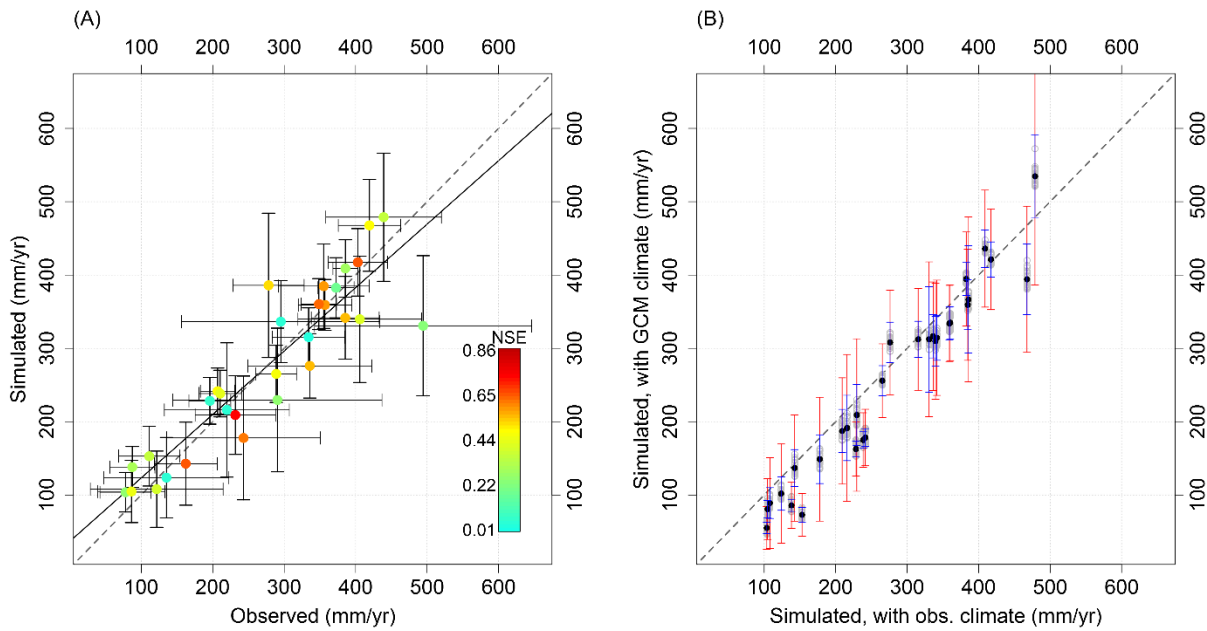
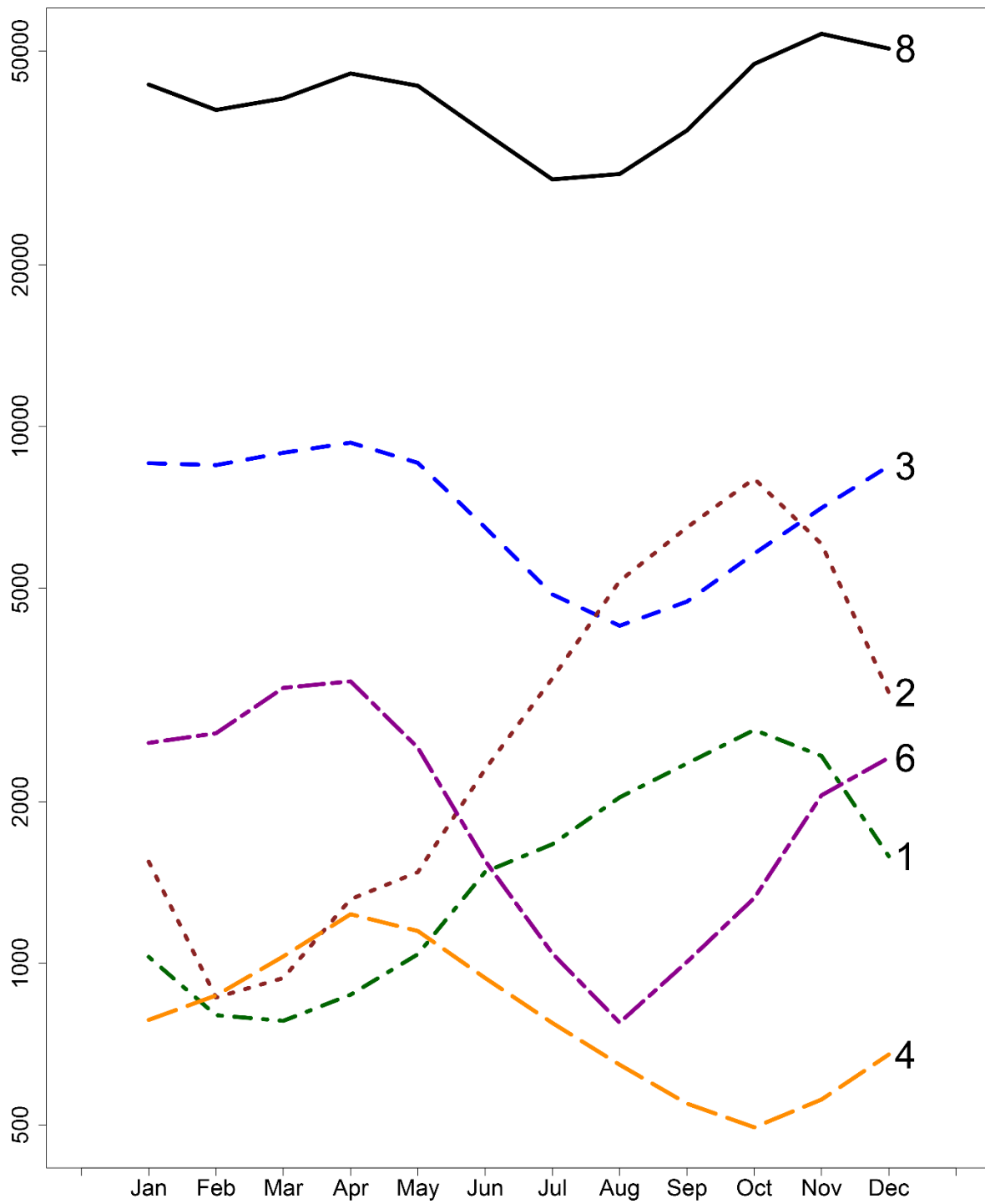


Figure 3. Comparison of observed and simulated annual runoff at the 30 streamflow gage locations (shown in Figure 1).

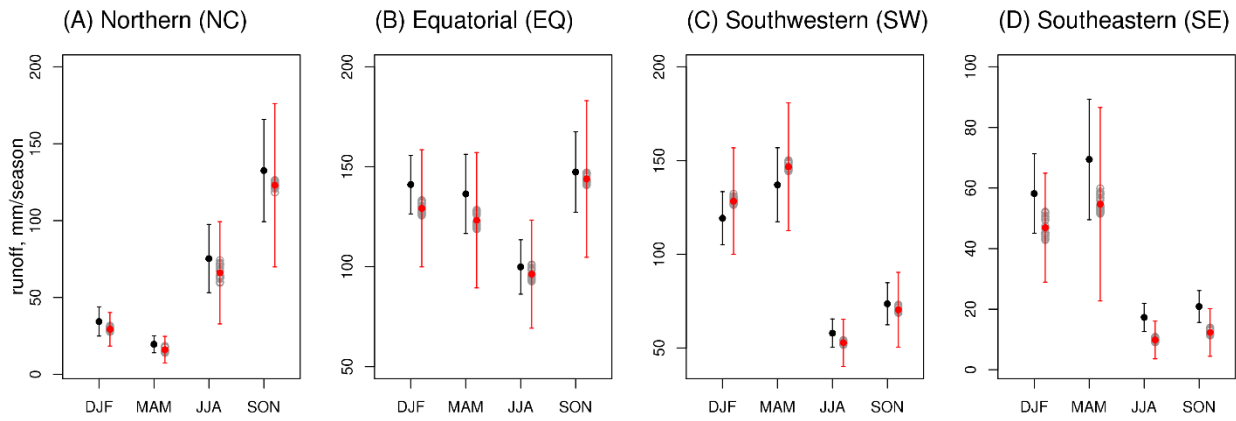
(A) Historical simulations with observed climate: the positions of the colored dots compare annual values of observed and simulated historical runoff; the dots' colors (see legend) show the Nash-Sutcliffe coefficient of efficiency (NSE) of observed vs. simulated monthly stream flows; and the black horizontal and vertical bars show observed and modeled inter-annual variability (\pm one standard deviation), respectively. The black line is linear regression fit between annual simulated and observed runoff ($y = 0.865 \pm 0.158x + 36.63, p < 0.001, R^2 = 0.82$), parameter bounds are the 95% confidence interval. (B) Simulations in the historical period with GCM-simulated climate: black dots show the multi-model mean; red (blue) vertical bars show modeled (forced with GCM-simulated historical climate) maximum (minimum) inter-annual variability (\pm one standard deviation) within the 25 simulations; and gray circles show multi-year mean of individual GCM simulations. The gray dotted lines in A and B are 1:1 line. The GCM-simulated forcings are statistically downscaled and bias-corrected.



37

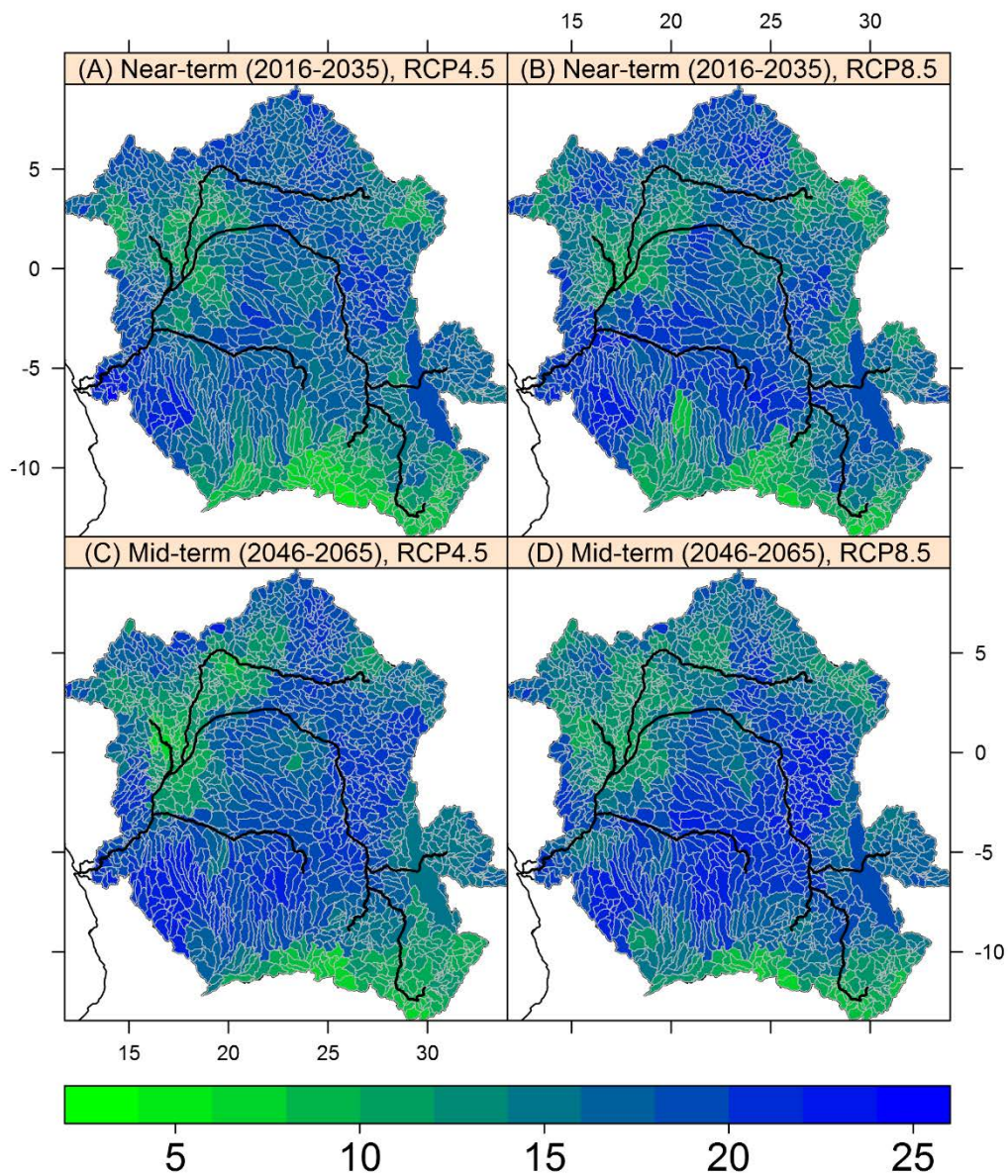
38 Figure 4 Mean monthly flows at selected tributaries in the CRB. Flows are in m³/s and gage numbers are identified in
 39 Figure 1. Monthly values are based on simulated flows (forced with observed precipitation) for the period 1950-2005.

40



41
 42 Figure 5 Seasonal variation in runoff in (A) Northern, (B) Equatorial, (C) Southwestern and (D) Southeastern Congo
 43 River Basin. Black dots and vertical bars show the modeled inter-annual variability forced with observed climate, red dots
 44 show the multi-model mean forced with GCM-simulated climate, red vertical bars show the maximum range of inter-
 45 annual variability within the 25 models and the grey open circles show the mean of individual models in the historical
 46 period, 1950-2005. Y-axis scale is different for each plot.

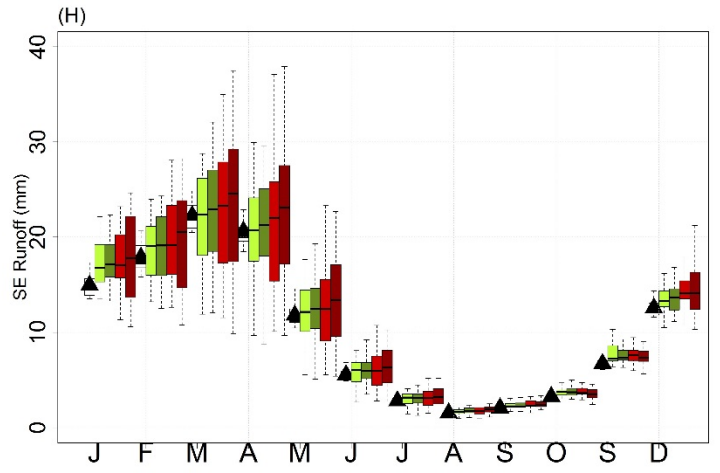
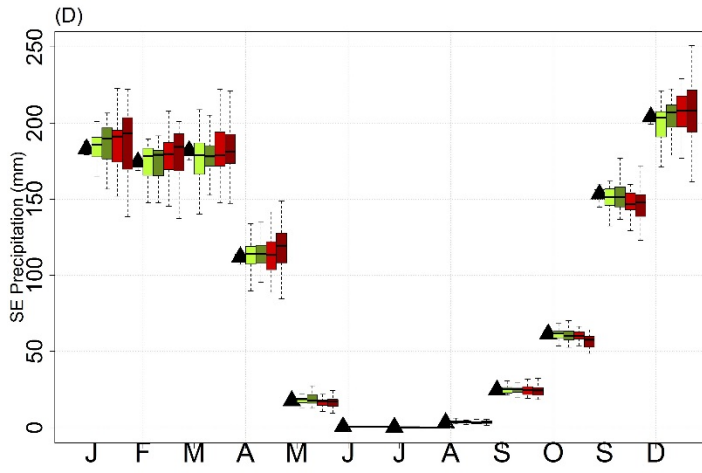
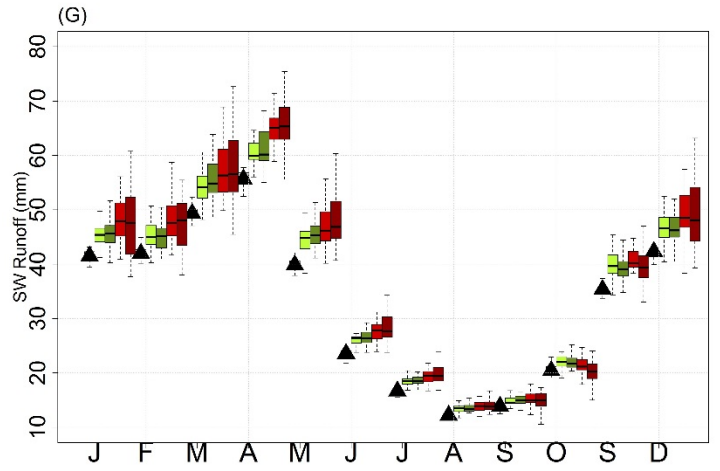
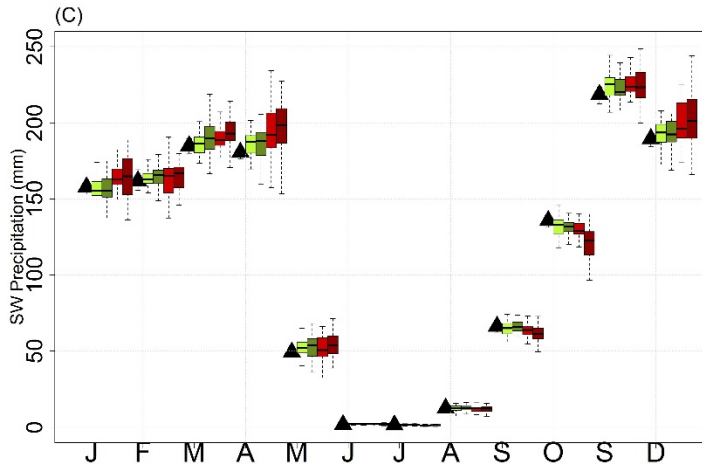
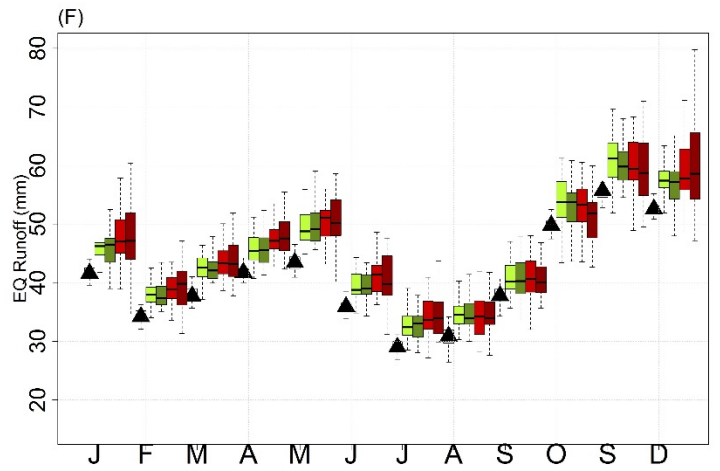
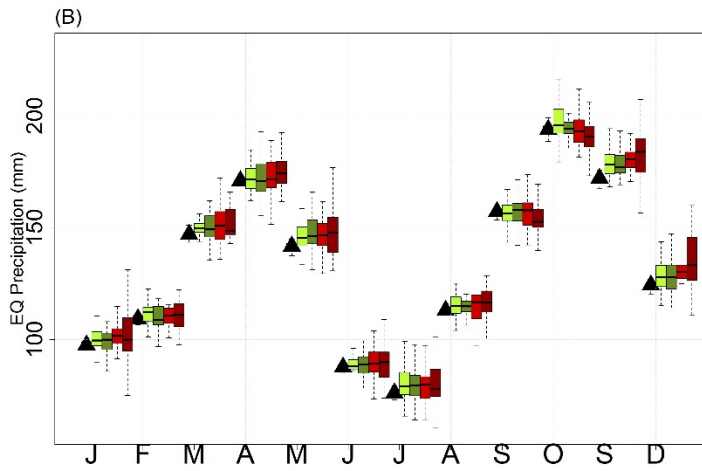
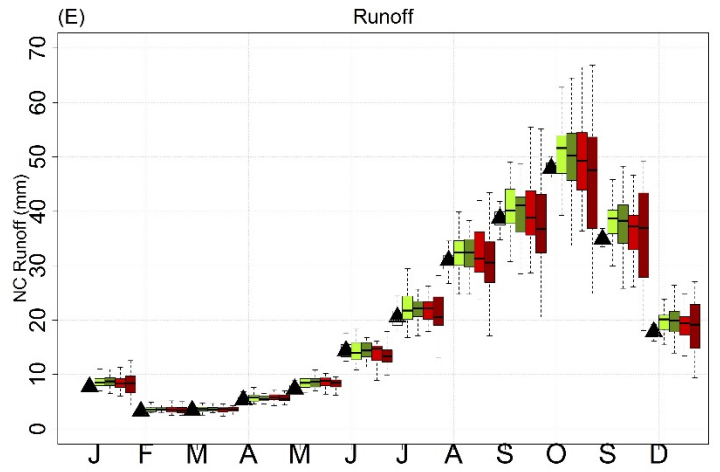
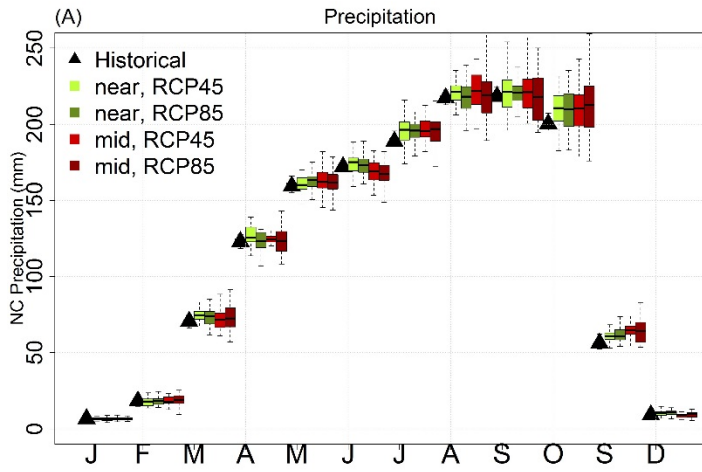
47



48

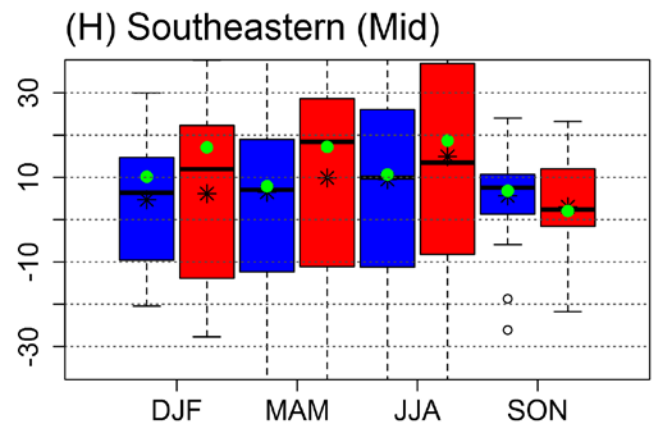
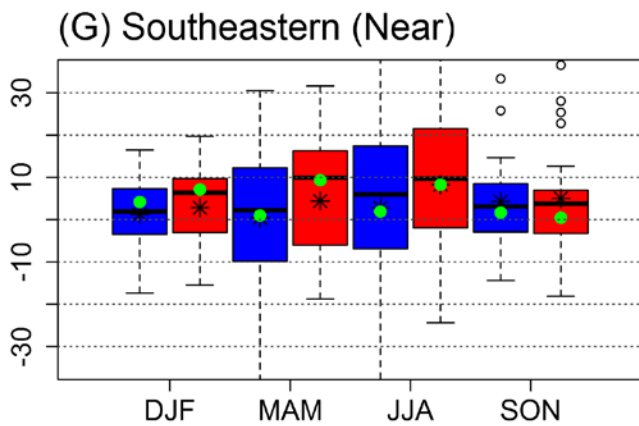
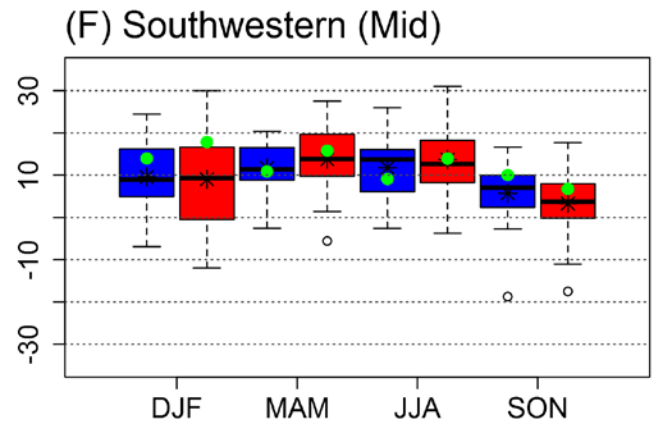
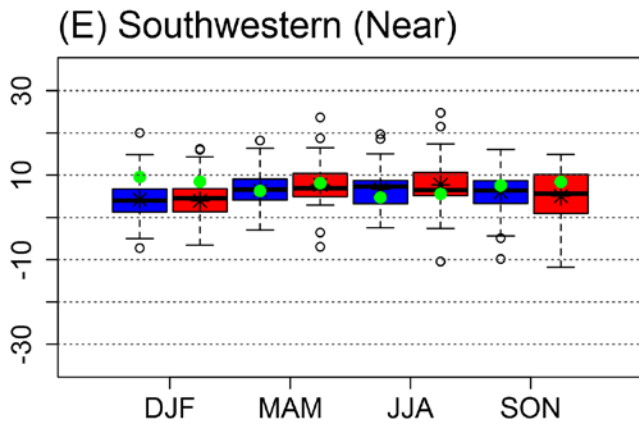
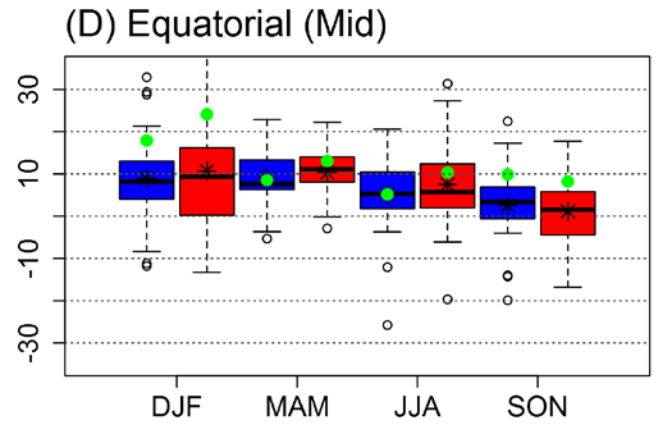
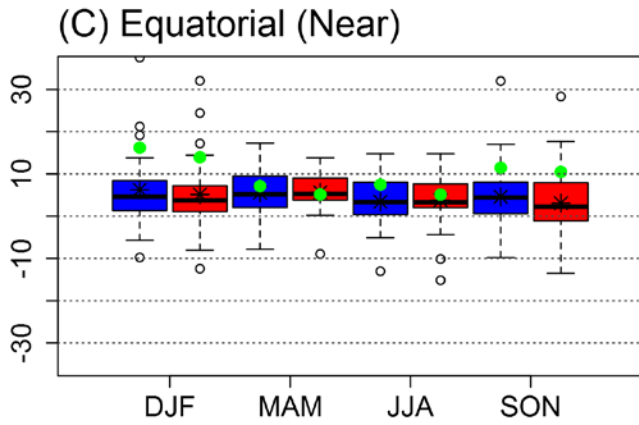
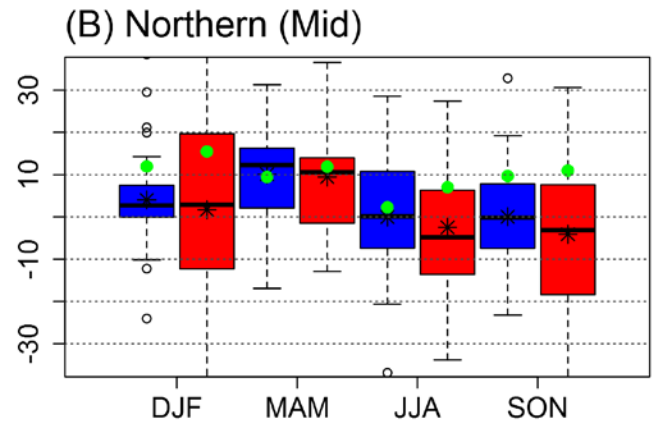
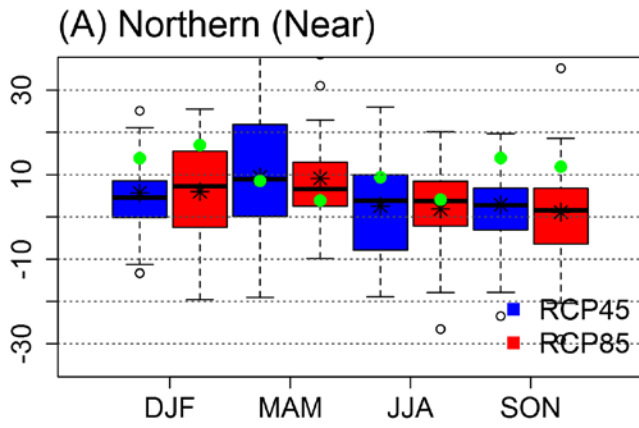
49 Figure 6 Number of climate model outputs that projects an increase in precipitation in the (A) near-term, 2016-2035,
 50 RCP4.5, (B) near-term RCP8.5, (C) mid-term, 2046-2065, RCP4.5 and (D) mid-term RCP8.5. Number of modeled
 51 precipitation outputs used is 25. Main rivers and lakes are also shown.

52



54 Figure 7 Monthly variation of precipitation (A-D) and runoff (E-H) in the four regions shown in Figure 1. Box-and-
55 whiskers for each month shows the inter-model variability for the historical period (black), near-term RCP4.5 (light
56 green), near-term RCP85 (dark green), mid-term RCP4.5 (red) and mid-term RCP8.5 (brown). The upper and lower end
57 of the boxes show the 75th and 25th quartiles, the mid bar in each box shows the median, and the outer lines cover
58 approximately 90% of the values. The multi-model mean value for the reference period is shown as triangles for clarity.
59 All values are in mm/month. NC – northern, EQ – equatorial, SE – southeast and SW – southwest, see Figure 1 for
60 locations.

61



62

63

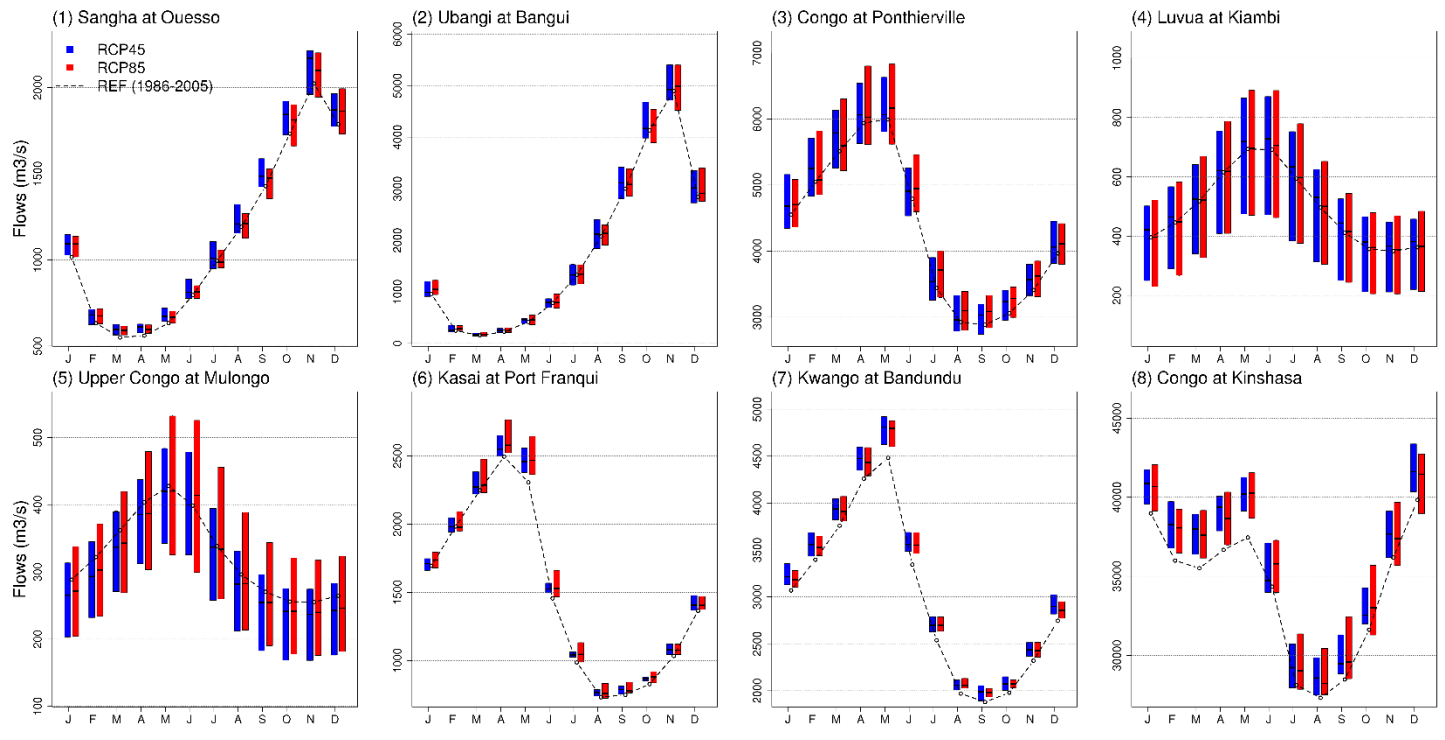
Figure 8 Seasonal runoff projections (as percent relative to the reference period 1986-2005) for the near-term (2016-2035)

64

and mid-term (2046-2065) projection period for northern (A-B), equatorial (C-D), southwestern (E-F) and southeastern

65 (G-H) regions. Boxes show the 25th and 75th percentiles, the horizontal line within the boxes show median value and the
 66 whiskers mark the 5th and 95th percentiles. The multi-model mean (asterisks) and the select-model mean (green dots) are
 67 also shown. The y-axis range is limited to show the smaller boxes. Y-axis values are in percentages.

68
 69
 70



71
 72
 73
 74
 75
 76

Figure 9 Accessible streamflow hydrographs in the near-term at selected locations shown in Figure 1A. Blue (red) bars show the inter-model variability. Dotted black line shows the hydrograph in the reference period (1986-2005). Figure numbers 1-8 coincide with the gage numbers in Figure 1.

77 **Tables in the main text**

78

79 Table 1 Global Climate Models whose outputs are used in this study. Further details about comparison of model outputs
80 and key references for GCMs are given in Aloysius et al., 2016.

Model Number	Model Name
M1	ACCESS1-3
M2	bcc-csm1-1
M3	BNU-ESM
M4	CanESM2
M5	CCSM4
M6	CESM1-CAM5
M7	CNRM-CM5
M8	CSIRO-Mk3-6-0
M9	EC-EARTH
M10	FIO-ESM
M[11-13]*	GISS-E2-H*
M[14-16]*	GISS-E2-R*
M17	HadGEM2-CC
M18	HadGEM2-ES
M19	INM-CM4
M20	IPSL-CM5A-LR
M21	MIROC5
M22	MIROC-ESM

M23 MPI-ESM-LR

M24 MRI-CGCM3

M25 NorESM1-M

81 * These climate models provide outputs from three different physics ensembles. We treat each a separate model.

82

84 Table 2 Multi-model mean of projected changes in precipitation (%) in the four regions within the Congo River Basin (see
 85 Figure 1) for the near-term (2016-2035) and the mid-term (2046-2065) relative to the reference period of 1986-2005. The
 86 regions are identified in Figure 1. The standard deviation values across the 25 GCM-simulations are provided in
 87 parenthesis. DJF: Dec-Jan-Feb, MAM: Mar-Apr-May, JJA: Jun-Jul-Aug and SON: Sep-Oct-Nov.

	Northern (NC)		Equatorial (EQ)		Southwestern (SW)		Southeastern (SE)	
	RCP4.5	RCP8.5	RCP4.5	RCP8.5	RCP4.5	RCP8.5	RCP4.5	RCP8.5
<u>Near future (2016-2035)</u>								
Annual	1.6 (3.0)	1.3 (2.9)	1.3 (2.9)	1.1 (2.7)	1.3 (2.3)	1.5 (2.6)	-0.4 (3.7)	0.1 (4.2)
DJF	3.3 (13.3)	5.4 (21)	2.0 (4.9)	1.4 (4.7)	1.6 (3.2)	1.8 (4.0)	-0.3 (3.7)	0.04 (4.8)
MAM	1.4 (4.5)	1.1 (3.7)	0.5 (2.9)	0.8 (2.8)	1.5 (4.2)	2.5 (5.2)	-0.5 (7.8)	0.9 (8.3)
JJA	1.3 (3.3)	0.4 (4.2)	1.3 (4.2)	1.3 (4.7)	-0.7 (14.6)	-0.3 (15.7)	19.6 (32.0)	18.7 (31.6)
SON	2.3 (4.6)	2.3 (4.7)	1.7 (4.1)	1.1 (4.0)	0.9 (3.6)	0.2 (3.8)	-0.6 (5.4)	-1 (4.8)
<u>Mid-term (2046-2065)</u>								
Annual	1.6 (3.8)	1.2 (4.9)	1.7 (3.4)	2.4 (3.9)	2.9 (2.9)	3.3 (4.0)	0.2 (5.4)	0.3 (7.4)
DJF	1.1 (15.2)	3.9 (18.8)	3.5 (6.3)	5.3 (9.4)	4.8 (5.1)	5.4 (7.4)	1.5 (6.4)	1.4 (9.6)
MAM	0.9 (4.4)	0.6 (5.4)	1.5 (3.5)	2.4 (3.5)	4.1 (5.1)	6.9 (5.8)	0.4 (9.6)	2 (11.0)
JJA	0.6 (4.3)	0.1 (5.5)	0.7 (5.8)	2.2 (7.3)	-6.1 (14.8)	-5.9 (19)	6.7 (30.6)	9.7 (32.0)
SON	3.4 (6.2)	2.9 (7.3)	1.3 (4.0)	0.6 (4.1)	-0.3 (4.2)	-2.5 (4.6)	-3.2 (5.2)	-4.6 (5.8)

90 Table 3 Multi-model mean of projected changes in runoff (%) in the four regions within the Congo River Basin for the
 91 near-term (2016-2035) and the mid-term (2046-2065) relative to the reference period of 1986-2005. The regions are
 92 identified in Figure 1. The standard deviation values across the 25 GCM-simulations are provided in parenthesis. The
 93 asterisks (*) show the degree of agreement that projected runoff > 0 in more than 50% of the ensembles. DJF: Dec-Jan-
 94 Feb, MAM: Mar-Apr-May, JJA: Jun-Jul-Aug and SON: Sep-Oct-Nov.

	Northern (NC)		Equatorial (EQ)		Southwestern (SW)		Southeastern (SE)	
	RCP4.5	RCP8.5	RCP4.5	RCP8.5	RCP4.5	RCP8.5	RCP4.5	RCP8.5
<u>Near future (2016-2035)</u>								
Annual	3.6 (12.1)	2.5 (11.2)	5.0 (7.0)*	4.3 (6.7)*	5.6 (4.8)*	6.0 (5.4)*	1.4 (12.8)	4.2 (12.1)
DJF	5.7 (13.3)	6.0 (14.1)	6.2 (9.8)*	5.1 (9.5)*	4.2 (6.1)*	3.9 (6.4)*	1.3 (9.3)	2.8 (9.8)
MAM	9.4 (15.0)*	9.1 (11.1)*	5.5 (6.3)*	5.7 (4.9)*	6.3 (5.1)*	7.7 (6.3)*	0.4 (18.4)	4.4 (17.3)
JJA	2.6 (12.1)	1.9 (10.2)	3.4 (6.3)*	3.8 (6.9)*	6.7 (5.5)*	7.7 (7.1)*	2.8 (20.7)	8.3 (19.6)
SON	2.8 (13.5)	1.1 (13.3)	4.6 (9.1)*	3.1 (9.4)	6.0 (6.4)*	5.0 (6.4)*	4.3 (10.7)	5.0 (12.6)
<u>Mid-term (2046-2065)</u>								
Annual	1.2 (15.4)	-2.0 (17.1)	6.3 (8.1)*	7.2 (8.5)*	9.9 (5.9)*	10.4 (8.2)	6.1 (18.8)	8.3 (20.6)
DJF	4.0 (18.0)	1.7 (21.9)	8.9 (11.2)*	10.7 (14.7)*	9.6 (7.9)*	9.0 (12.4)	4.7 (14.9)	6.2 (20.3)
MAM	10.1 (13.4)*	9.5 (17.1)	8.9 (7.1)*	10.3 (6.2)*	11.7 (6.1)*	13.7 (8.0)*	6.5 (26.2)	9.9 (26.6)
JJA	-0.02 (14.5)	-2.5 (15.8)	5.2 (9.8)*	7.5 (11)*	11.8 (7.1)*	13.7 (8.6)*	9.5 (25.9)	14.9 (25.7)
SON	0.04 (17.7)	-4.1 (19.4)	2.5 (9.3)*	1.1 (8.5)	5.7 (7.2)*	3.3 (7.7)	5.6 (11.2)*	3.1 (12.6)

95

96